On Characterizing and Simulating Porous Media

Problem Presenters

Zhenyu He, Vasu Venkateshwaran, Gore

Report Editor

David A. Edwards, University of Delaware

Thirty-Third Annual Workshop on Mathematical Problems in Industry
June 19–23, 2017
New Jersey Institute of Technology

Table of Contents

Preface

At the 33rd Annual Workshop on Mathematical Problems in Industry (MPI), Zhenyu He and Vasu Venkateshwaran of Gore presented a problem concerning the modeling of particle flow through a multi-layer porous media filter.

This manuscript is really a collection of reports from teams in the group working on several aspects of the problem. Here is a brief summary of each:

1. Chen *et al.* outline the general problem, and introduce a discrete model for the porous media. They present simulations of a multiply-connected multiple-layer model.
2. Bi *et al.* present simulations of a singly-connected multiple-layer discrete model.
3. Edwards *et al.* derive a continuous model for the porous media, and present some analytical and numerical results in special cases.
4. Using a continuous model, Allaire *et al.* numerically analyze the performance of a double-layer filter as the widths of the two layers vary.
5. Using a continuous model, Sun *et al.* numerically analyze the performance of a three-layer filter: two wide layers with a thin transition layer sandwiched between. They look at how to optimize filtration using characteristics of these layers.

In addition to the authors of these reports, the following people participated in the group discussions:

- Shuchi Agarwal, University of Delhi
- Manuchehr Aminian, University of North Carolina, Chapel Hill
- Daniel Fong, United States Merchant Marine Academy
- Binan Gu, New Jersey Institute of Technology
- Qingxia Li, Fisk University
- Don Schwendeman, Rensselaer Polytechnic Institute
- Jake Taylor-King, Oxford University

Special recognition is due to Jake Taylor-King, Anqi Chen, Joe Gaone, and Tin Phan for making the group's oral presentations throughout the week.

A General Introduction; Multiply-Connected Discrete Model

Anqi Chen, Michigan State University
David A. Edwards, University of Delaware
Joe Gaone, Worcester Polytechnic Institute

Section 1: Introduction

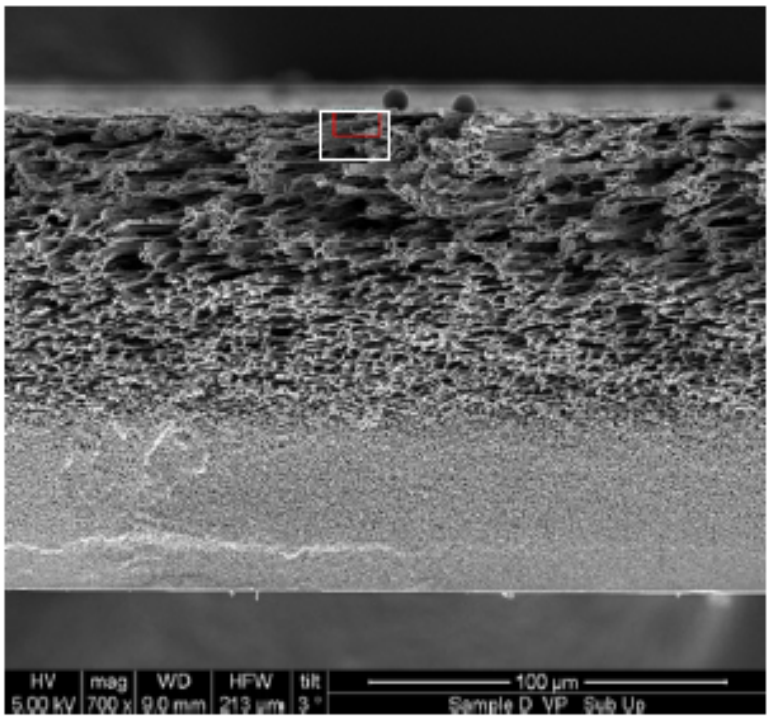

Figure 1.1. Picture of layered filter [1]. Here the particles enter at the top, and exit at the bottom. Note the variation in pore size from top to bottom, as well as the large particles adhering to the top.

Consider a liquid mixture of solid particles in solution (for instance, water). We consider the filtration of these particles by a filter made of a porous medium. If the pores in the filter have a size distribution with a small variance, the particles tend to clump together and clog the filters at the point of entry. (See §2.1 of "Porous Media: Continuous Model" or the chapter by Allaire *et al.*)

Therefore, it is desirable to design porous media which consist of a wider range of pore sizes in order to increase the effective area used for filtration. One simple way to construct such filters is to stack layers on top of each other, with the mean pore radius decreasing from large at the layers near the entrance to small at the layers near the exit (see Fig. 1.1).

At the workshop, the larger group analyzed various models (both discrete and continuous) for this situation. It is our hope that the analysis of such problems will provide Gore with inspirations to design more effective filters.

In this particular report, we analyze a discrete model for the pore structure. We show how a heterogeneous filtered can be mathematically assembled from multiple layers with similar properties.

Section 2: Two-Dimensional Discrete Model, Particle Transport

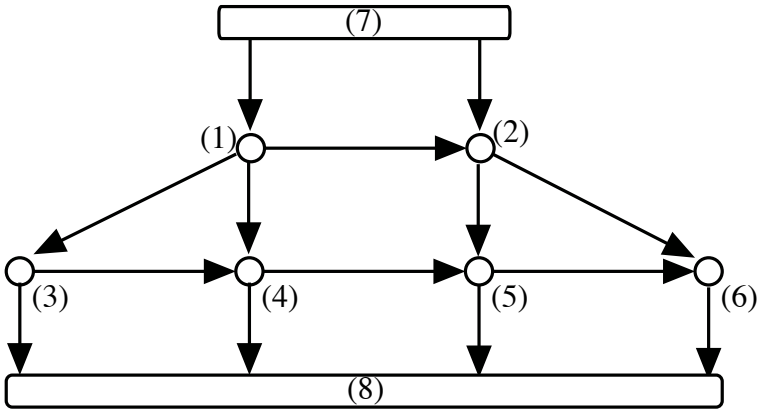

Figure 2.1. Two-layer model: $y_{\max} = 1$, $x_{\max} = 2$, $s = 2$.

We model the porous matrix as a directed graph or network, as shown in Fig. 2.1. Here the top corresponds to the flow entrance, and the bottom corresponds to the flow exit. As a first approximation, we consider the matrix to be two-dimensional.

We extend the analysis in section 4.1 of [2], to which the interested reader is referred for further details. Each edge represents a pore connecting two nodes, which are denoted with parentheses (replacing the bar notation in [2]). The direction of the edge corresponds to a positive flow (or pressure drop). Note that this is simplify a mathematical construct; if in the true system the fluid flowed from node (2) to node (1) in Fig. 2.1, the flow would have a negative value since it flows in the direction opposite to the arrow.

As it represents a pore, each edge i has a number d_i associated with it, which corresponds to the diameter of the associated pore. (This can also be thought of as a capacity for the edge.) The d_i are chosen to come from a particular probability distribution (see the next section for more details). In [2], the authors consider a two-dimensional model where the diameter of each pore came from the same distribution.

We now extend their analysis in the following manner (see Fig. 2.1):

1. We consider a single coarse layer sitting atop a single fine layer.
   - This will later be extended to the case where the number of layers L is greater than 2.)
2. The coarse layer consists of $y_{\max}$ rows (N in [2]) of $x_{\max}$ nodes each (M in [2]). The fine layer also consists of $y_{\max}$ rows, but with $sx_{\max}$ nodes each.
   - There is no requirement that the number of rows be the same in each layer—we consider this case in this report for simplicity.

- Similarly, there is no reason why the *scale factor* s must be the same between each layer; again, we just consider this case for simplicity.

3. Each of the $x_{\max}$ nodes in the bottom row of the coarse layer connects to exactly s nodes in the top row of the fine layer.
   - Such an assumption would be consistent with the type of filter shown in Fig. 1.1. However, one could imagine a filter made up of different layers simply laid on top of one another. A discrete network for such a filter would have a different connection structure, as described in the next chapter by Chen *et al.*

Fig. 2.1 illustrates the case with $y_{\max} = 1$, $x_{\max} = 2$, $s = 2$.

For later computational simplicity, as we label the nodes, we must keep the interior nodes together as a group, and the source and sink together as a group. We use the particular algorithm as outlined below. Nodes are numbered consecutively starting at the upper left, so:

- the first row in the coarse layer contains nodes (1) through ($x_{\max}$), the second row in the coarse layer contains nodes ($x_{\max} + 1$) through ($2x_{\max}$), and the last row in the coarse layer contains nodes $y_{\max}(x_{\max} - 1) + 1$ through ($y_{\max}x_{\max}$).
- the first row in the fine layer contains nodes ($y_{\max}x_{\max} + 1$) through ($x_{\max}(y_{\max} + s)$), the second row in the fine layer contains nodes ($x_{\max}(y_{\max} + s) + 1$) through ($x_{\max}(y_{\max}+2s)$), and the last row in the fine layer contains nodes ($x_{\max}((s+1)y_{\max} - s) + 1$) through ($y_{\max}x_{\max}(s + 1)$).
- after the last row in the fine layer, we append a source node numbered ($y_{\max}x_{\max}(s + 1) + 1$).
- the sink node is labeled last as (J), $J \equiv y_{\max}x_{\max}(s + 1) + 2$.

Importantly, note that all the interior nodes are numbered first. Moreover, we have $J_{\mathrm{i}} = y_{\max}x_{\max}(s + 1)$ interior nodes, where the subscript "i" refers to "interior".

The labeling of the edges is not as important, and Matlab can handle it automatically. Therefore, we just count them:

- there are $y_{\max}(x_{\max} - 1)$ horizontal edges in the coarse layer, and $y_{\max}(sx_{\max} - 1)$ horizontal edges in the fine layer.
- there are $y_{\max}x_{\max}$ vertical edges *ending* in the coarse layer (including the edges originating in the source), and $sy_{\max}x_{\max}$ vertical edges *beginning* in the fine layer (including the edges ending in the sink).
- there are $sx_{\max}$ vertical edges leading from the coarse layer to the fine layer.

Hence the total number of edges is

$$\begin{aligned} I &\equiv y_{\max}(x_{\max} - 1) + y_{\max}(sx_{\max} - 1) + y_{\max}x_{\max} + sy_{\max}x_{\max} + sx_{\max} \\ &= x_{\max}(2(s + 1)y_{\max} + s) - 2y_{\max}. \end{aligned}$$

Given this directed graph, we may create the *incidence matrix* $D \in \mathcal{R}^{I \times J}$ as follows:

$$D_{i(j)} = \begin{cases} -1, & \text{if edge } i \text{ points away from node } (j), \\ 1, & \text{if edge } i \text{ points toward node } (j), \\ 0, & \text{if edge } i \text{ does not connect to node } (j). \end{cases} \tag{2.1}$$

(Here we use capital letters for the entries of the incidence matrix instead of small letters to avoid confusion with the diameter, below.)

Now we use the incidence matrix to solve for the flows in each edge and the pressure drop in each node. Let $p_{(j)}$ be the pressure in node (j), and let $(\Delta p)_i$ be the difference in pressure across edge i, which connects nodes (j_1) and (j_2). But then

$$(\Delta p)_i = p_{(j_2)} - p_{(j_1)} = \sum_{j=1}^{J} D_{i(j)} p_{(j)}, \tag{2.2}$$

as all the other $D_{i(j)} = 0$. But this is just the ith row of the following expression:

$$\mathbf{\Delta p} = D\mathbf{p}, \qquad \mathbf{\Delta p} \in \mathcal{R}^I, \quad \mathbf{p} \in \mathcal{R}^J. \tag{2.3}$$

We may use a similar calculation to relate the volume flux Q_i through edge i and the net volume flux $q_{(j)}$ through node (j). In particular,

$$q_{(j)} = (\text{sum of fluxes in}) - (\text{sum of fluxes out}) = \sum_{i=1}^{I} D_{i(j)} Q_i,$$

as all the other $D_{i(j)} = 0$. But this is just the jth row of the following expression:

$$\mathbf{q} = D^T \mathbf{Q}, \qquad \mathbf{q} \in \mathcal{R}^J, \quad \mathbf{Q} \in \mathcal{R}^I. \tag{2.4}$$

Using a normalized form of the Hagen-Poiseuille Law [3], we have that the flow through each node is given by

$$Q_i = -d_i^4 (\Delta p)_i. \tag{2.5}$$

(More discussion of the distribution of the d_i will be discussed in the next section.) Writing in matrix form, we have

$$\mathbf{Q} = R^{-1} \mathbf{\Delta p}, \qquad \mathbf{Q} \in \mathcal{R}^I, \quad R \in \mathcal{R}^{I \times I}, \tag{2.6a}$$

where R^{-1} is the inverse of the *resistance matrix*. R^{-1} is a diagonal matrix with

$$(R^{-1})_{ii} = -d_i^4. \tag{2.6b}$$

With these expressions in hand, we may eliminate the variables corresponding to the edges and reduce to an expression that just contains variables corresponding to the edges. Substituting (2.6a) into (2.3), we obtain

$$\mathbf{Q} = R^{-1} D \mathbf{p}. \tag{2.7}$$

Substituting (2.7) into (2.4), we obtain

$$\mathbf{q} = D^T(R^{-1}D\mathbf{p}) = L\mathbf{p}, \tag{2.8a}$$

where $L \in \mathcal{R}^{J\times J}$, the *Laplacian matrix*, is given by

$$L = D^T R^{-1} D. \tag{2.8b}$$

Note that the Laplacian matrix is symmetric.

Now we exploit the cumbersome numbering system defined above. We know that the net flux through any interior node is zero. But these nodes are all numbered first, so we may rewrite (2.8a) in the following partitioned form:

$$\begin{pmatrix} \mathbf{0} \\ \mathbf{q}_\mathrm{s} \end{pmatrix} = \begin{pmatrix} A & B^T \\ B & C \end{pmatrix} \begin{pmatrix} \mathbf{p}_\mathrm{i} \\ \mathbf{p}_\mathrm{s} \end{pmatrix}, \tag{2.9}$$

where $\mathbf{0}$ and $\mathbf{p}_\mathrm{i} \in \mathcal{R}^{J_\mathrm{i}}$, $\mathbf{p}_\mathrm{s}$ and $\mathbf{q}_\mathrm{s} \in \mathcal{R}^2$, $A \in \mathcal{R}^{J_\mathrm{i}\times J_\mathrm{i}}$, $B \in \mathcal{R}^{J_\mathrm{i}\times 2}$, and $C \in \mathcal{R}^{2\times 2}$. Moreover, note that A and C are symmetric.

Expanding the first row of (2.9), we obtain

$$\begin{aligned} \mathbf{0} &= A\mathbf{p}_\mathrm{i} + B^T\mathbf{p}_\mathrm{s} \\ \mathbf{p}_\mathrm{i} &= -A^{-1}B^T\mathbf{p}_\mathrm{s}. \end{aligned} \tag{2.10}$$

But $\mathbf{p}_\mathrm{s}$ is known, for the pressure is assumed to be 0 at the sinks, and p_0 at the source. (In the code, we take $p_0 = 1$.) Therefore, we have

$$\mathbf{p}_\mathrm{i} = -A^{-1}B^T \begin{pmatrix} 1 \\ 0 \end{pmatrix}.$$

Once we have $\mathbf{p}_\mathrm{i}$, we may calculate $\mathbf{Q}$ from (2.7) and $\mathbf{q}_\mathrm{s}$ from the second row of (2.9):

$$\mathbf{q}_\mathrm{s} = B\mathbf{p}_\mathrm{i} + C\mathbf{p}_\mathrm{s}. \tag{2.11}$$

Next we want to trace a particle's path through the porous medium. We repeat the analysis in section 4.3 in [2], as the discussion in section 2 of this work allows us to use the analysis directly. We define $P_{(k)(j)}$ to be the probability that a particle travels directly from node (j) to node (k) along some edge k. We set this probability equal to the proportion of the total flux from node (j) that arrives at node (k):

$$P_{(k)(j)} = \begin{cases} \dfrac{\text{outward flux from } (j) \text{ to } (k) \text{ along edge } i}{\text{total outward flux from } (j)}, & \text{total outward flux from } (j) \neq 0, \\ 0, & \text{else.} \end{cases} \tag{2.12}$$

To calculate the numerator of (2.12), we see that if there is a positive flux from (j) along edge i, that means that either:

- edge i is oriented away from (j), in which case $Q_i > 0$ and $D_{i(j)} = -1$
- edge i is oriented toward (j), in which case $Q_i < 0$ and $D_{i(j)} = 1$

If the sign of Q_i is reversed, we have a net inward flux to (j) along edge i, which contributes nothing to the numerator. Hence we have that the outward flux from (j) along edge i is given by $\max\{-D_{i(j)}Q_i, 0\}$. And edge i connects (j) and (k) if $|D_{i(k)}| = 1$. Hence the term in the numerator is

$$S_{(j)(k)} = \sum_{i=1}^{I} |D_{i(k)}| \max\{-D_{i(j)}Q_i, 0\}, \quad j \neq k. \tag{2.13a}$$

Why the restriction? Well, if $j = k$, then we are counting *every* edge that emanates from (j), so

$$S_{(j)(j)} = \sum_{i=1}^{I} |D_{i(j)}| \max\{-D_{i(j)}Q_i, 0\} \tag{2.13b}$$

becomes the denominator of (2.12). How can we calculate S? Note that $D_{i(j)}Q_i$ is the ijth component of ΛD, where Λ is a diagonal matrix in $\mathcal{R}^{I\times I}$ with

$$\Lambda_{ii} = Q_i. \tag{2.14}$$

With this definition, then the sums in (2.13) define

$$S = (\max\{-\Lambda D, O\})^T |D|,$$

where we have to keep in mind that (k) is the first index, and the maximum is computed componentwise.

Then if the sums in (2.13) define a matrix S, then

$$P_{(k)(j)} = \begin{cases} \dfrac{S_{(j)(k)}}{S_{(j)(j)}} - \delta_{(j)(k)}, & S_{(j)(j)} \neq 0, \\ 0, & \text{else}, \end{cases} \tag{2.15}$$

where δ represents the Kronecker delta function, and is used to ensure that $P_{(j)(j)} = 0$. Note also that we have to take the transpose again.

Once this is calculated, we can create a clogging simulation as in section 4.7.1 of [2] using the following algorithm. Consider a particle of diameter d_p.

1. The particle starts at the source, so set $(j) = (J-1)$.
2. Choose a node (k) to which the particle will travel using the probability distribution in (2.15), and determine the corresponding edge number i.
3. If $d_\mathrm{p} < d_i$, the particle passes through the pore.
   (a) If $(k) = (J)$ (the sink node), the particle has escaped. Return to step #1.
   (b) Otherwise set $(j) = (k)$ and go to step #2.
4. If $d_\mathrm{p} \geq d_i$, the particle clogs the pore.
   (a) Set $d_i = 0$, which means from (2.5) that there will never be flow through edge i again.
   (b) Since d_i has changed, so will R^{-1}. Using that new value, calculate $\mathbf{p}_i$ and $\mathbf{Q}$.
   (c) If $\mathbf{Q} \neq \mathbf{0}$, calculate $P_{(k)(j)}$ and start another particle at step #1. Otherwise, the entire filter is clogged.

Section 3: Two-Dimensional Discrete Model, Pore and Particle Sizes

Now that we have an algorithm in place to propagate particles through the simulated filter, it remains to choose d_{p} and d_{i}. For the purposes of this report, we choose the pore sizes to have a gamma distribution:

$$d_i \sim \Gamma(k, \theta) \qquad \Longrightarrow \qquad \mathrm{E}[d_i] = k\theta, \qquad \mathrm{Var}[d_i] = k\theta^2. \tag{3.1}$$

At first, the particle size was taken to be fixed, and we treat just a single layer. This allows us to compare our code with computations in [2], as well as to understand the basic transport dynamics in the porous medium before adding the complication of additional layers.

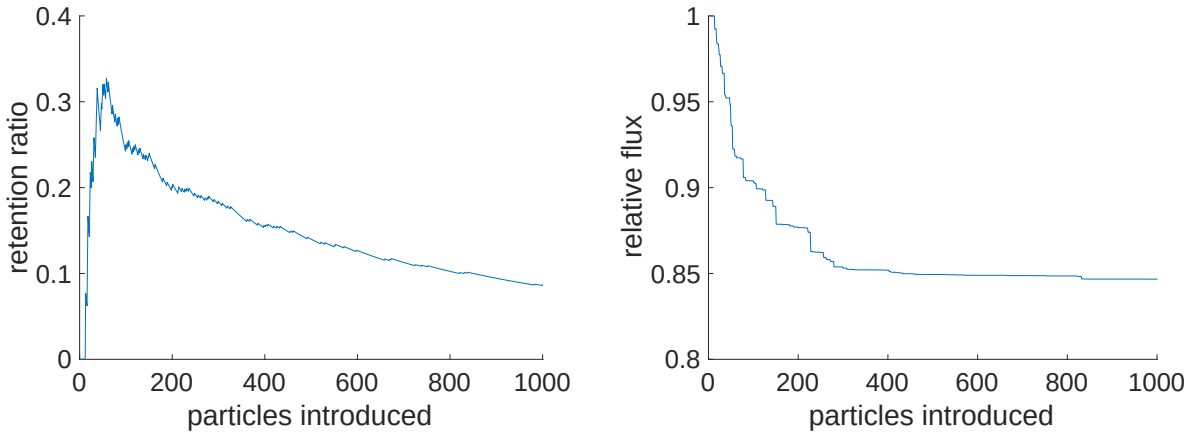

Figure 3.1. One-layer model, $d_{\mathrm{p}} = 0.05$, $d_i \sim \Gamma(2, 0.0475)$, $y_{\max} = 10$, $x_{\max} = 30$.

Results from a test case with a single layer are shown in Fig. 3.1; the parameters indicate a mean pore size about double the particle size. Note that with these parameters, small pores will be clogged by the particles, while larger pores continue to transport particles.

Note that in this case, the flux graph is concave up. Initially, there is a relatively high number of small pores that the particles can clog, so the flux decays quickly. However, as time passes, the number of (cloggable) small pores decays as a proportion of all remaining open pores, so the flux rate decays more slowly, eventually reaching a horizontal asymptote. Moreover, the retention ratio will asymptote to 0 (as the molecules stop being trapped).

Next we considered the more realistic case where the particle sizes also follow a probability distribition. For the one-layer model, we took the particle sizes to follow the same

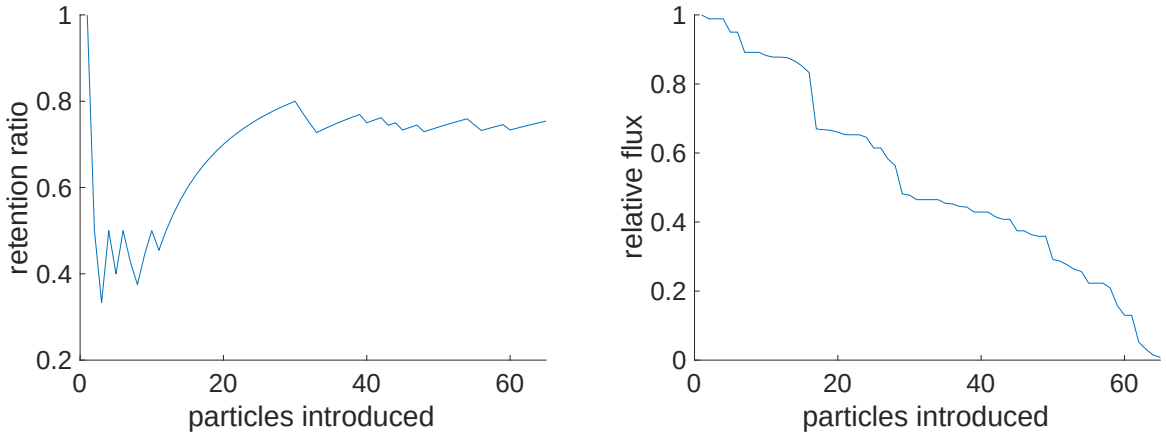

Figure 3.2. One-layer model, $d_{\mathrm{p}}, d_i \sim \Gamma(2, 0.0475)$, $y_{\max} = 10$, $x_{\max} = 30$.

probability distribution as the pores, but the underlying code is general enough to handle other situations.

Results from a test case with a single layer are shown in Fig. 3.2. Note that with these parameters, it is highly likely that some particles will be larger than the pores. Hence the filter completely clogs very quickly. (Compare the horizontal axes in Figs. 3.1 and 3.2.) We postulate that the number of particles needed to clog the filter should scale with $x_{\max}$, as that's how many pores (in a single row) it would take to shut the flow down completely.

Since both the pores and the particles come from the same distribution, at any time we would expect the probability of a pore being clogged to be roughly the same, which yields a retention rate graph which asymptotes to a fixed value. This is also consistent with the flux graph, which decays relatively uniformly over the experiment. The goal for a well-designed filter is to have a high flow rate (with high retention ratio) for almost all of its life cycle, followed by a quick collapse as clogging occurs. This would correspond to a flux graph which is concave down.

With the addition of another layer, the question then becomes as to how to assign the pore diameters in the various layers. In particular, we would like the total pore cross-sectional area in each layer to be roughly comparable. Therefore, since we have s times as many nodes in the second layer, we would like the expected value of a single pore *area* to be a factor of s smaller, so we would like the expected value of a single pore *diameter* to be a factor of $s^{1/2}$ smaller. Similarly, we would like the *variance* of the diameter to be smaller by the same factor of s. Hence we have

$$d_i(\text{layer } l) \sim \Gamma\left(\frac{k}{s^{(l-1)/2}}, \theta\right)$$

$$\mathrm{E}[d_i(\text{layer } l)] = \frac{k\theta}{s^{(l-1)/2}}, \qquad \mathrm{Var}[d_i(\text{layer } l)] = \frac{k\theta^2}{s^{(l-1)/2}}, \tag{3.2}$$

where the layers are numbered from top to bottom.

For the pores that connect the layers, we first use the geometric mean of the scale

factors for the layers being connected:

$$d_i(\text{layer } l \text{ to layer } l+1) \sim \Gamma\left(\frac{k}{s^{(2l-1)/4}}, \theta\right), \tag{3.3}$$

Then the question remains as to how to distribute the particle sizes in the multiple-layer case. Suppose that we have L layers. Then the geometric mean of the mean pore sizes of the finest two layers is given by

$$\left[\left(\frac{k\theta}{s^{(L-1)/2}}\right)\left(\frac{k\theta}{s^{(L-2)/2}}\right)\right]^{1/2} = \frac{k\theta}{s^{(2L-3)/4}} = \frac{\mathrm{E}[d_i(\text{layer } 1)]}{s^{(2L-3)/4}}.$$

Therefore, we reduce the fixed size by a comparable factor to keep the ratio of particle size to geometric mean of the finest two layers constant:

$$d_\mathrm{p}(L \text{ layers}) = \frac{d_\mathrm{p}(\text{one layer})}{s^{(2L-3)/4}}. \tag{3.4}$$

We stress that this choice was made just for testing and presenting the comparisons in the manuscript; the code is robust enough to handle any value of d_p.

Results from a test case are shown in Fig. 3.3. Note that with the new scaling in (3.4), the particles are the same size relative to the pores *connecting* the layers, which means they are larger relative to the finer layer as compared with the one-layer case. Therefore, smaller pores will be clogged by the particles, while larger pores continue to transport particles. Hence the flux will asymptote to a finite value (as the larger pores will never be clogged), and the retention ratio will asymptote to 0 (as the molecules stop being trapped).

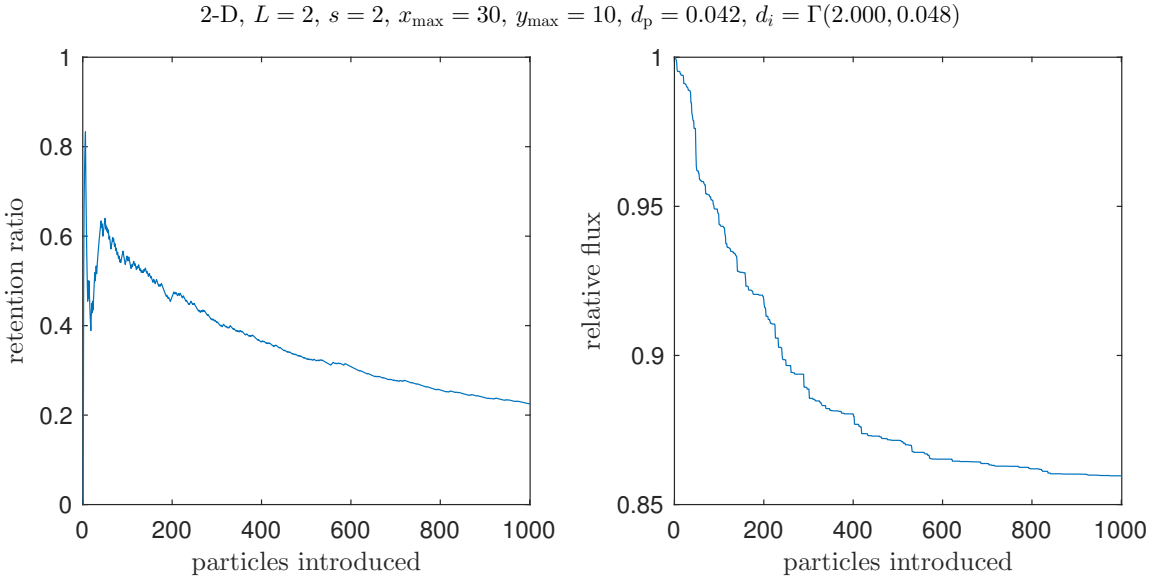

Figure 3.3. Two-layer model, d_p fixed, $s = 2$.

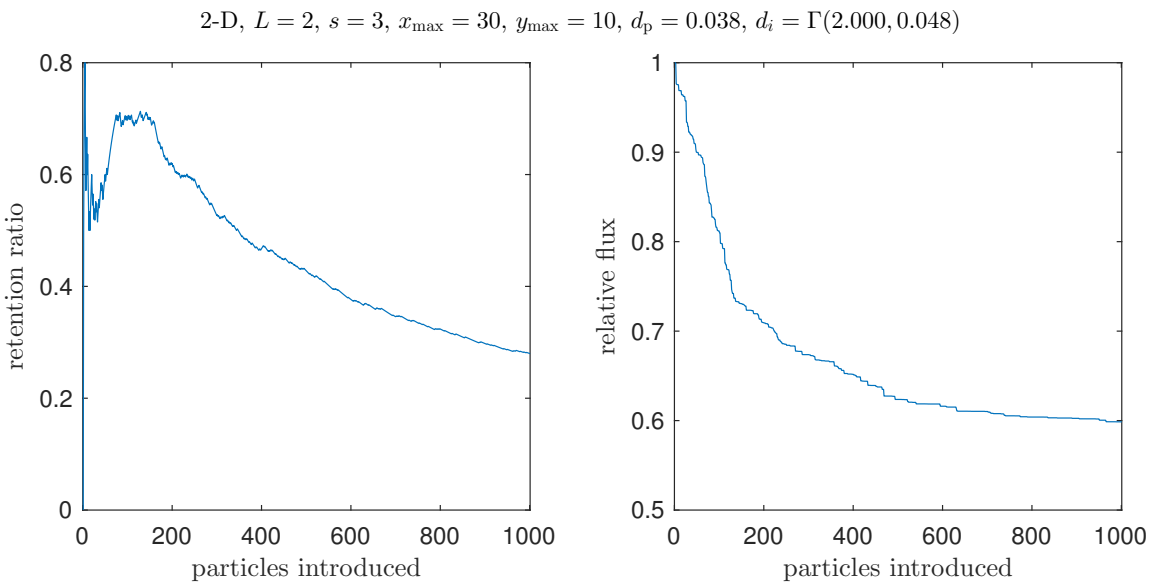

Figure 3.4. Two-layer model, d_{p} fixed, $s = 3$.

Moreover, in comparison with the one-layer case, we would expect the flux to be less, since the particles are larger compared with the finer mesh, which would then cause the retention ratio to decreases more slowly, since there are more pores that can be clogged. Though this is not clear from the simulations with $s = 2$, it does show up in Figure 3.4, which illustrates the case where the scale factor $s = 3$.

Motivated by the previous discussion, in the case of a variable particle size, we again reduce the mean and variance by the same factor:

$$d_{\mathrm{p}} \sim \Gamma\left(\frac{k}{s^{(2L-3)/4}}, \theta\right) \qquad \Longrightarrow \qquad \mathrm{E}[d_{\mathrm{p}}] = \frac{k\theta}{s^{(2L-3)/4}}, \qquad \mathrm{Var}[d_{\mathrm{p}}] = \frac{k\theta^2}{s^{(2L-3)/4}}. \quad (3.5)$$

We stress that this choice was made just for testing and presenting the comparisons in the manuscript; the code is robust enough to handle any distribution of particle sizes, and is set up to easily handle a gamma distribution with any combination of parameters.

Results from a test case are shown in Fig. 3.5. Note that with these parameters, though the particles may pass through the coarse layer, it is highly like that the particles will be larger than the pores in the fine layer. Hence the filter again completely clogs. However, it takes longer, since there are now s times as many pores in the finer portion of the filter. In particular, we see that as particles are first introduced, any resultant clogging does not affect the flux very much. Hence we get a flux graph which is more concave down, as desired.

This behavior is even more pronounced as the scale factor increases, as shown in Figure 3.6. Note that in all three cases shown with varying particle sizes (Figs. 3.2, 3.5, and 3.6), the retention ratio stays roughly the same.

We then expand to 3 layers; the results are shown in Figs. 3.7 and 3.8, which exhibit the same qualitative behavior as the two-layer case. Hence introducing additional layers should not affect the solution as much as increasing the scale factor, *as long as* the particles are then resized as in (3.4) of (3.5).

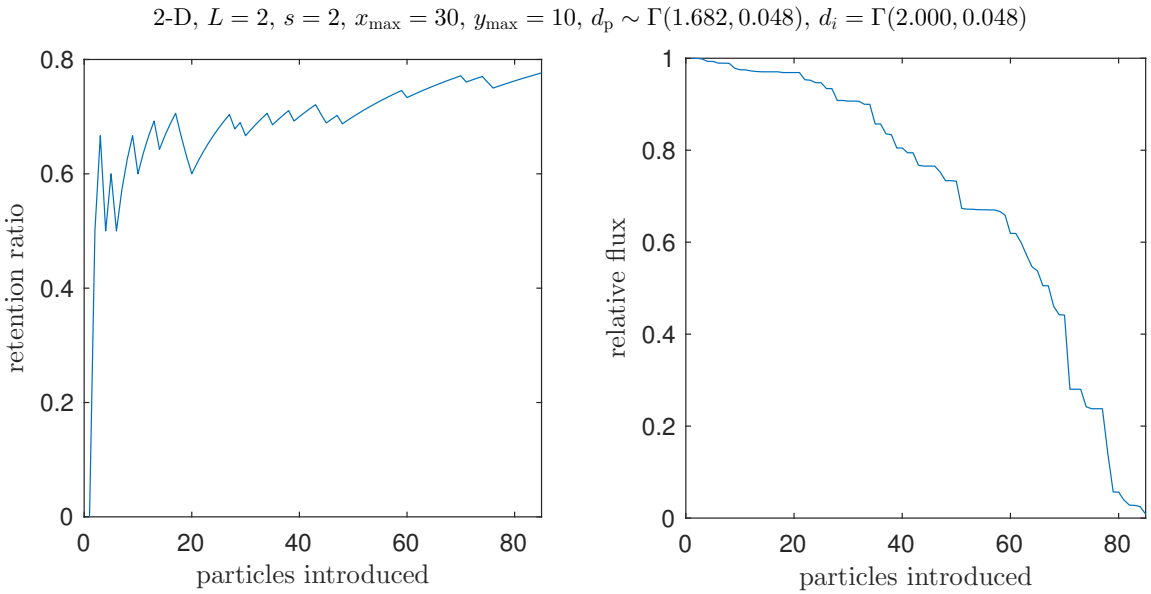

Figure 3.5. Two-layer model, d_{p} varies, $s = 2$.

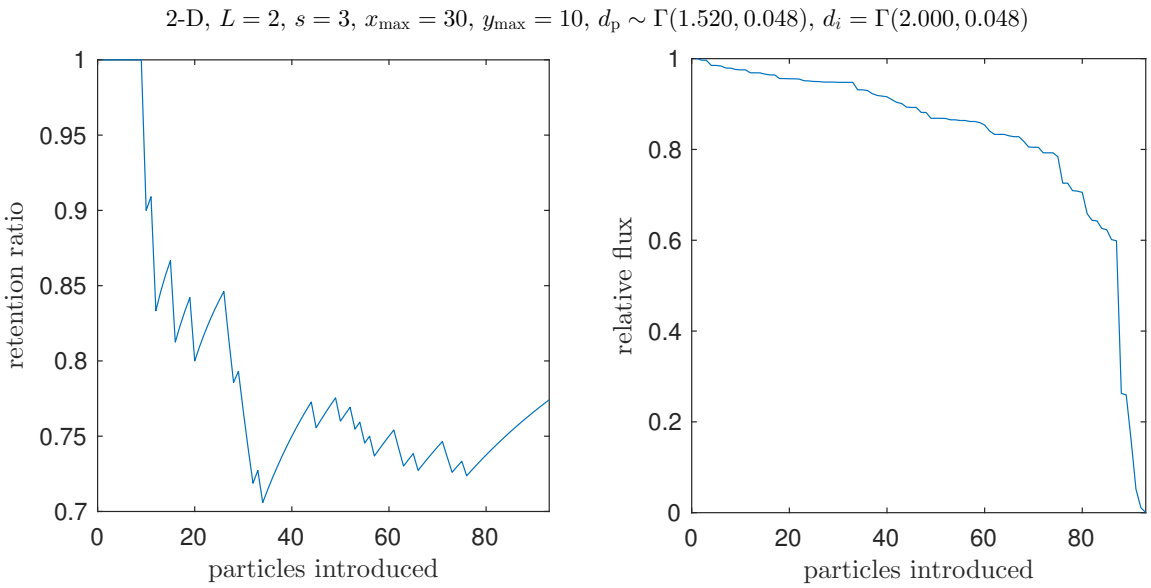

Figure 3.6. Two-layer model, d_{p} varies, $s = 3$.

One quantitative difference between the two- and three-layer case can be seen in the flux graphs for the distributed pore size case. In particular, we see that the number of particles needed to clog the filter in the three-layer case is larger than for the two-layer case. This is because there are now s^2 more nodes in the finest layer than in the coarsest layer, which means it takes more particles to clog a row of the finest layer.

Another possibility for the pores that connect the layers is to use the *arithemtic* mean of the scale factors for the layers being connected:

$$d_i(\text{layer } l \text{ to layer } l+1) \sim \Gamma\left(\frac{k}{2s^{(l-1)/2}} + \frac{k}{2s^{l/2}}, \theta\right), \tag{3.6}$$

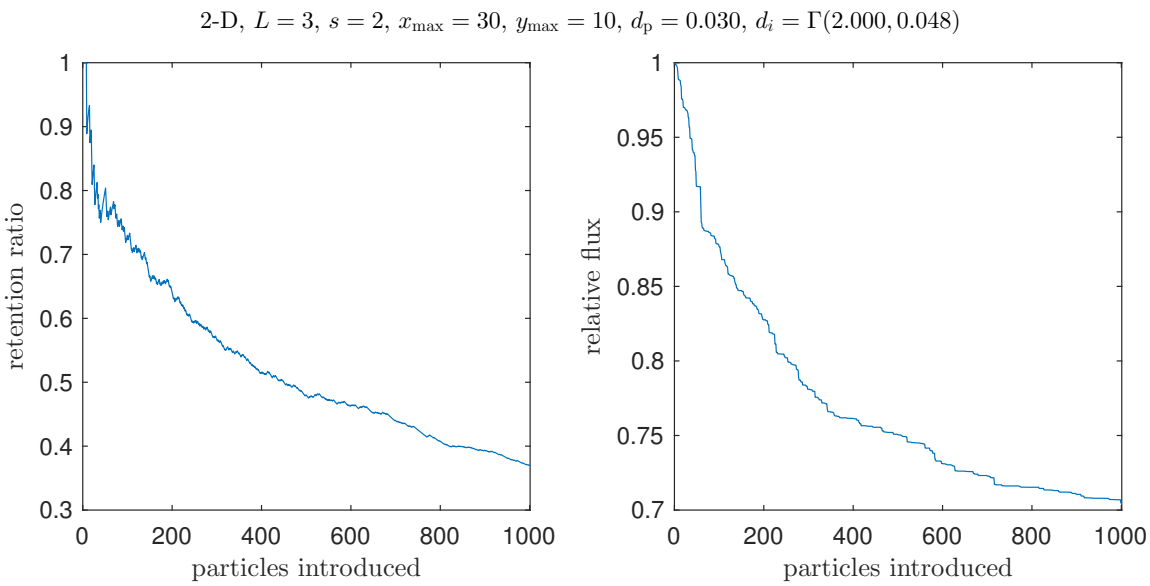

Figure 3.7. Three-layer model, d_{p} fixed, $s = 2$.

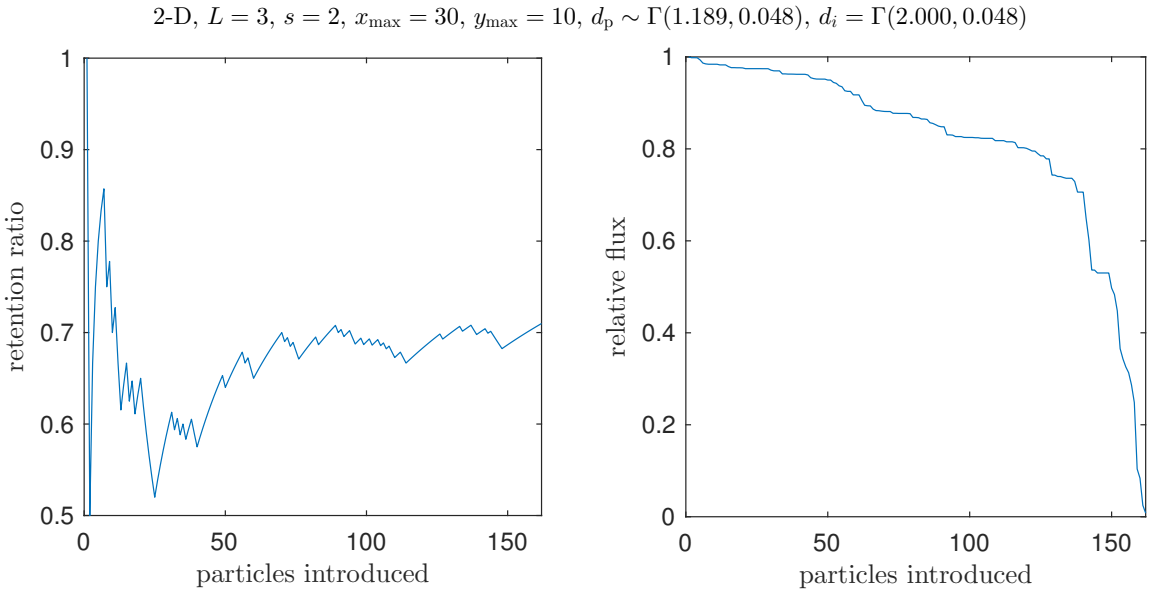

Figure 3.8. Three-layer model, d_{p} varies, $s = 2$.

which replaces (3.3). Results are shown in Figs. 3.9 and 3.10, which indicate that the choice of mean used does not appreciably affect the flux or retention rate.

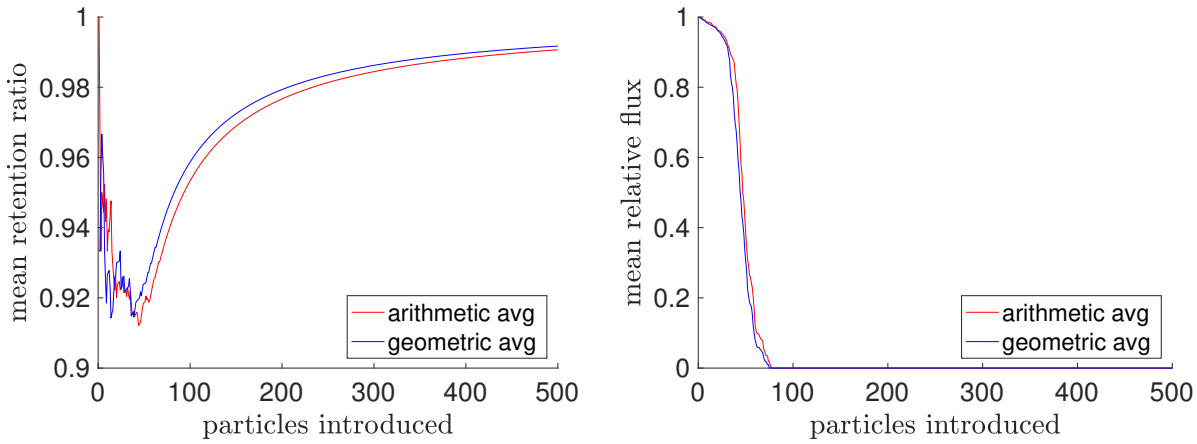

Figure 3.9. Comparison of means for two-layer model.

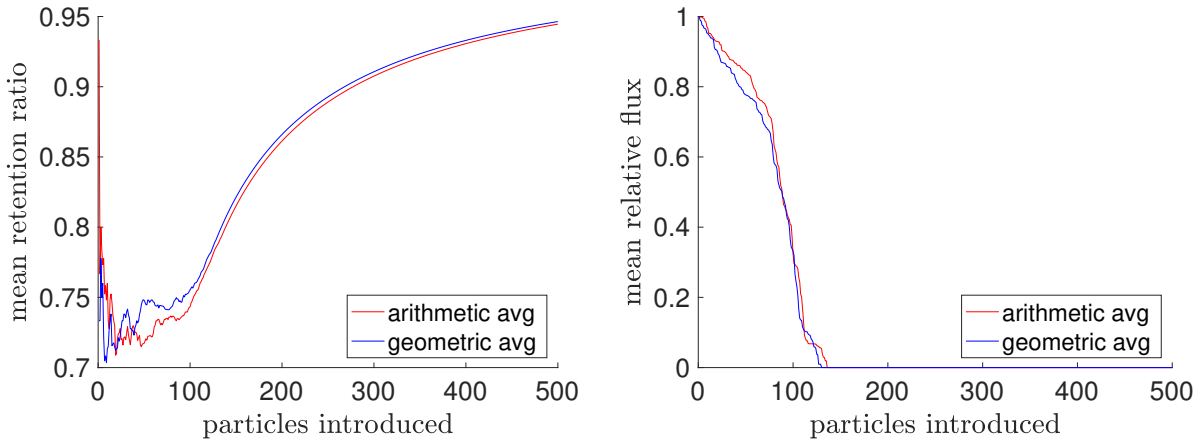

Figure 3.10. Comparison of means for three-layer model.

Section 4: Three-Dimensional Discrete Model

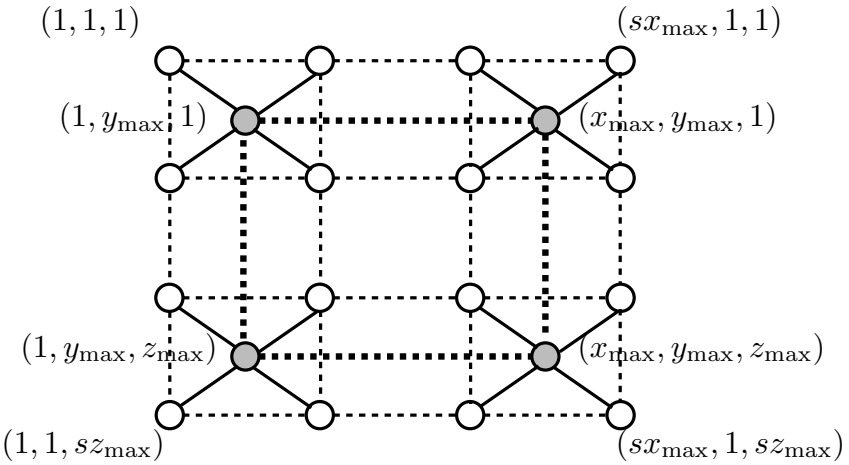

Figure 4.1. Three-dimensional two-layer model: view from above. $y_{\max} = 1$, $x_{\max} = 2$, $z_{\max} = 2$, $s = 2$. Solid circles: nodes in coarse layer. Open circles: nodes in fine layer. Dotted lines: edges within layers. Solid lines: edges between layers.

We next examine the case of a three-dimensional model. In this case each layer is a lattice of size $x_{\max}$ by $z_{\max}$ (see Fig. 4.1, though note there is no reason why $x_{\max}$ and $z_{\max}$ have to be equal). Here are the major differences between the 2-D and 3-D models.

- In Matlab it is easiest to give (x, y, z) coordinates to each node, then assign them sequentially to a vector in order to create D. This is illustrated in Fig. 4.1; note that each layer will have its own coordinate system.
- Since we now have s^2 more nodes in the fine layer than the coarse layer (in the two layer case), we reduce the mean pore *area* in the fine layer by a factor of s^2, which means a reduction in the pore *diameter* by s. Hence (3.2)–(3.5) become

$$d_i(\text{layer } l) \sim \Gamma\left(\frac{k}{s^{l-1}}, \theta\right) \quad \Longrightarrow \quad \mathrm{E}[d_i(\text{layer } l)] = \frac{k\theta}{s^{l-1}}, \quad \mathrm{Var}[d_i(\text{layer } l)] = \frac{k\theta^2}{s^{l-1}}, \tag{4.1}$$

$$d_i(\text{layer } l \text{ to layer } l+1) \sim \Gamma\left(\frac{k}{s^{(2l-1)/2}}, \theta\right), \tag{4.2}$$

$$d_{\mathrm{p}}(L \text{ layers}) = \frac{d_{\mathrm{p}}(\text{one layer})}{s^{(2L-3)/2}}, \tag{4.3}$$

$$d_{\mathrm{p}} \sim \Gamma\left(\frac{k}{s^{(2L-3)/2}}, \theta\right) \qquad \Longrightarrow \qquad \mathrm{E}[d_{\mathrm{p}}] = \frac{k\theta}{s^{(2L-3)/2}}, \qquad \mathrm{Var}[d_{\mathrm{p}}] = \frac{k\theta^2}{s^{(2L-3)/2}}. \tag{4.4}$$

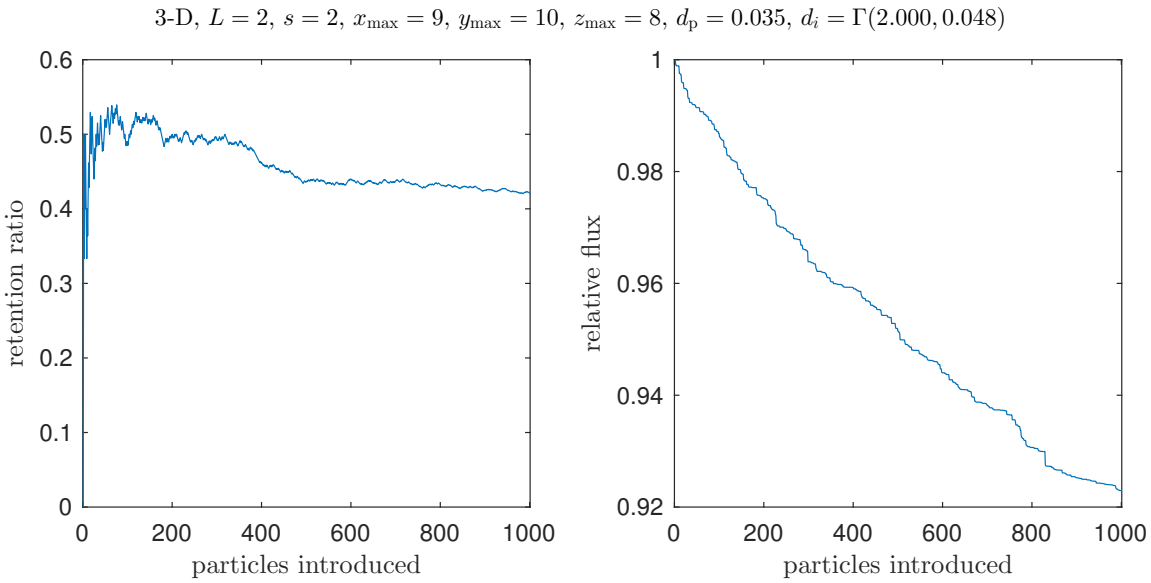

Figure 4.2. Two-layer model, d_{p} fixed.

Fig. 4.2 shows the case of constant particle size. Note that the same trends that occurred in the two-dimensional case occur here. However, we note that since there are now s^2 more nodes in the lower layer (with a correspondingly higher number of connecting pores), the number of pores to block is higher. Hence the flux decreases at a slower rate, and hence the decrease in the retention ratio is difficult to discern with only 1000 particles.

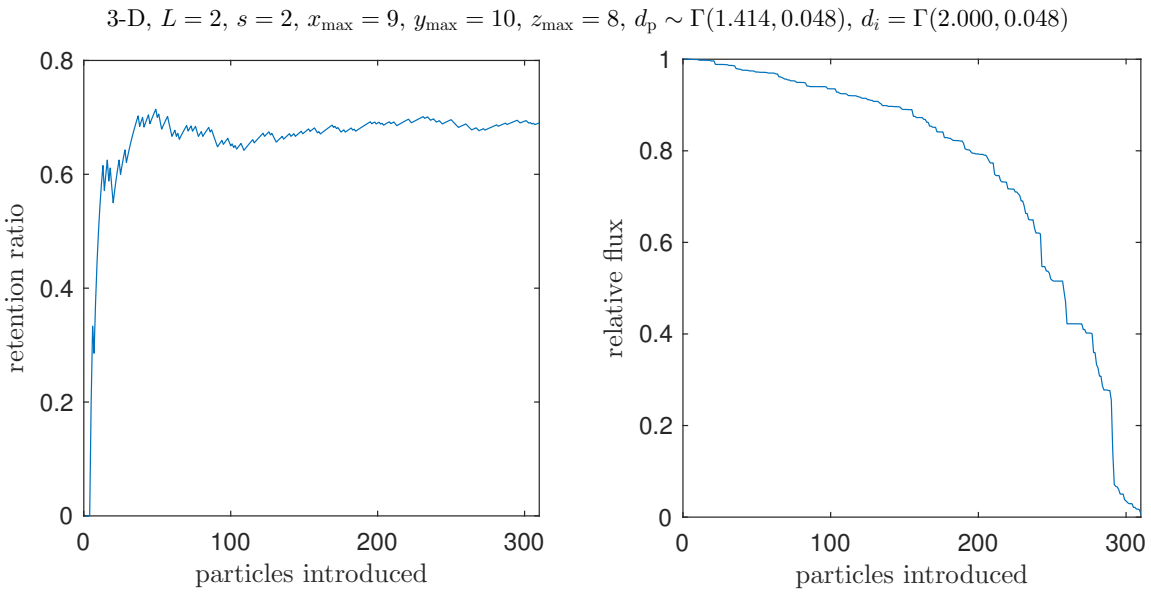

Figure 4.3. Two-layer model, d_{p} varies.

Fig. 4.3 shows the case of distributed particle size. Again the number of particles needed to clog the filter is larger because there are more pores.

Section 5: Conclusions and Further Research

When filtering particles through a porous medium with one typical pore size, the filter tends to clog at the inlet, thus wasting the media underneath. To rectify this problem, engineers construct filters made of layers of media, as shown in Fig. 1.1. With varying mean pore sizes in each layer, the filter more efficiently filters the particles. This is characterized by a high retention ratio and a flux graph which is concave down.

In this work we presented both two- and three-dimensional discrete models for such filters. Each pore is represented as an edge with varying capacity connecting two nodes. Flow through the network is modeled by the Hagen-Poiseuille law, and a pore is said to be clogged if its radius is smaller than the particle flowing through the network.

In this work, the pore diameters in each layer are modeled as given from a gamma distribution, and the particle diameters are either set as fixed or also coming from a gamma distribution. However, the underlying code is robust enough to handle other distributions of particle and pore sizes as needed.

At the interface between layers, each node in the coarser layer is assumed to connect to a larger set of nodes in the finer layer. This models layers that have relatively smooth transitions between the layer, as in Fig. 1.1. However, other models are possible for layers that are simply placed on top of each other; see the next chapter by Chen *et al.*

Our results indicate that if one constructs a filter where the mean particle size lies between the mean pore sizes of the two finest layers of the filter, a more effective filter (especially in terms of the flux graph) can be designed. The way one models the pore sizes of the connections between the layers seems to be irrelevant.

These simulations provide a direct way to simulate and visualize filtration through porous media. However, continuous models (as in the section by Breward *et al.*) are also useful to understand the underlying dynamics.

Nomenclature

A: block in partitioned form of L (2.9).
B: block in partitioned form of L (2.9).
C: block in partitioned form of L (2.9).
D: incidence matrix (2.1).
d: diameter of pore or particle (2.4).
I: total number of edges.
i: indexing variable for edges (2.1).
J: total number of nodes.
j: indexing variable for nodes (2.1).
k: indexing variable for nodes (2.12) or parameter in the gamma distribution (3.1).
L: Lagrangian matrix of (inferred) prices for each slot (2.8b) or total number of layers (3.4).
l: indexing variable for layers.
P: matrix of transition probabilities (2.12).
$\mathbf{p}$: vector of pressures in each node (2.3).
$\mathbf{Q}$: vector of volume fluxes through each pore (2.4).
$\mathbf{q}$: vector of volume fluxes through each node (2.4).
R: resistance matrix of (inferred) prices for each slot (2.6b).
S: matrix used in the computation of P (2.13a).
$x_{\max}$: number of nodes in one direction per row of coarse layer.
$y_{\max}$: number of rows per layer.
$z_{\max}$: number of nodes in the other direction per row of coarse layer in three-dimensional model.
$\mathbf{\Delta p}$: vector of pressure drop across pores (2.3).
Λ: diagonal matrix of the Q_i (2.14).
θ: parameter in the gamma distribution (3.1).

Other Notation

$(\cdot)$: denotes node $\cdot$.
i: as a subscript, refers to interior nodes.
p: as a subscript, refers to the particle.
s: as a subscript, refers to source or sink nodes nodes.

References

[1] W. Li, *Fouling Models for Optimizing Asymmetry of Microfiltration Membranes.* Cincinnati: University of Cincinnati, 2009.

[2] U. Beuscher, *et al.*, "Characterization of porous filtration media," in *Proceedings of the 25th Annual Workshop on Mathematical Problems in Industry*, 2009.

[3] F. Civan, *Porous Media Transport Phenomena.* Hoboken: Wiley, 2011.

Concatenation of several filters from single-filter building blocks

Anqi Chen
Michigan State University

Chuan Bi
University of Delaware

Taras Lakoba
University of Vermont

1 Introduction

The main idea of this approach is this: Use the already existing single-filter code as a building block and construct a multi-filter code using that building block with minimal changes inside it. Thus, we seek a way to concatenate two (or more) single-filter codes into a multi-filter one.

For brevity, we will explain the idea using the two-filter case. Generalizations will be described in later sections.

Simulation of the (multi-)filter's performance involves two steps:

1. Find the fluxes through the network with given properties and given the pressure drop, δP, across the filter.

2. Using these fluxes, simulate the passage of a particle through the network.

A straightforward concatenation of two single-filter codes in a two-filter code has two obstacles that one needs to overcome. First, while we are given the *total* pressure drop δP across both filters together, we do not know the pressure drops, δP_1 and δP_2, across each one of the individual filters. Thus, to enable the implementation of Step 1 of the above simulation algorithm, one needs to first find δP_1 and δP_2. Second, even if we are able to determine δP_1 and δP_2, we will need a strategy to redistribute the total flux from the output of Filter 1 into the input of Filter 2. In this report we will address, to various degrees of satisfaction, ways to overcome both of these obstacles.

In Section 2 we will present a method of finding δP_1 and δP_2 of two individual filters. This will address the first obstacle described above. As for the second obstacle, we will assume in Section 2 that the total output of Filter 1 is uniformly distributed into the input of Filter 2. A justification for that will be given. In Section 3 we will present implementation details of this method and simulation results obtained with it. In Section 4 we will outline how our method could be generalized to three or more filters, as well as how the assumption of the uniform distribution of Filter 1's output into Filter 2 could be modified (in a way other than simply prescribing a different distribution).

2 Concatenation of two filters

The total flux T through a given network is a given function of the applied pressure drop:

$$T = T(\delta P). \tag{1}$$

In the notations of the 2009 MPI report, $T = \sum_{i_{\rm top}} (q_c)_{i_{\rm top}}$, where $i_{\rm top}$ are the indices of the top layer in the network, and q_c is defined at the top of p. 9 of that report. It follows from Sec. 4.1 of that report that the function $T(\delta P)$ in (1) is linear (for a fixed network), with $T(0) = 0$. This has been verified by our simulations. Note that in doing so, one needs to use the same seed of the random number generator, which determines the properties of the network, when varying δP.

Suppose one concatenates two filters with the flux–pressure functions $T_1(\delta P)$ and $T_2(\delta P)$, and suppose that the output of Filter 1 is uniformly distributed into the input of Filter 2. Suppose also that the total pressure drop $\delta P_{\rm tot}$ over both filters together is known. Then the pressure drops $\delta P_{1,2}$ over Filters $1, 2$ are to satisfy two conditions:

$$T_1(\delta P_1) - T_2(\delta P_2) = 0, \tag{2a}$$

$$\delta P_1 + \delta P_2 = \delta P_{\rm tot}. \tag{2b}$$

Note that Eq. (2a) says that all of the output of Filter 1 goes in Filter 2.

Equations (2) form a system of 2 equations for 2 unknowns. If $T_{1,2}(\delta P)$ were general nonlinear functions, it could be solved iteratively by, say, the secant method. The situation, however, is even simpler: since $T_{1,2}(\delta P)$ are *linear* functions, then just two iterations of the secant method would give the exact solution of (2). Namely, suppose that two pairs, $(\delta P_1^{(1)}, \delta P_2^{(1)})$ and $(\delta P_1^{(2)}, \delta P_2^{(2)})$, are two (fairly arbitrary) guesses of the solution of (2). Then according to the secant method, the vector

$$\begin{pmatrix} \delta P_1^{(3)} \\ \delta P_2^{(3)} \end{pmatrix} = \begin{pmatrix} \delta P_1^{(2)} \\ \delta P_2^{(2)} \end{pmatrix} - J^{-1} \begin{pmatrix} T_1(\delta P_1^{(2)}) - T_2(\delta P_2^{(2)}) \\ \delta P_1^{(2)} + \delta P_2^{(2)} - \delta P_{\rm tot} \end{pmatrix}, \tag{3a}$$

where the Jacobian

$$J = \begin{pmatrix} \frac{T_1(\delta P_1^{(2)}) - T_1(\delta P_1^{(1)})}{\delta P_1^{(2)} - \delta P_1^{(1)}} & -\frac{T_2(\delta P_2^{(2)}) - T_2(\delta P_2^{(1)})}{\delta P_2^{(2)} - \delta P_2^{(1)}} \\ 1 & 1 \end{pmatrix}, \tag{3b}$$

is the exact solution of system (2).

The above process provides the values of the pressure drops over the individual filters, from which the single-filter code can determine the fluxes over each filter. Once a particle sent through this network blocks it, the network's configuration changes, and the fluxes are to be re-calculated, just as in the single-filter code.

Remark 1 Recall that the above procedure assumes that the total output (flux) of Filter 1 is aggregated into one number, $T_1(\delta P_1)$, and then evenly distributed into the nodes of Filter 2's input layer. (Of course, the even distribution can be replaced with any other distribution.) This simple idea should produce the same *average* result as the combined filter built (somehow) of the two networks, and also *averaged* over a large number of random realizations of the network. This is because the properties of the filter are assumed to be uniform in the direction transverse to the flux, and the random structure of the bottom filter is in no way related to that of the top filter.

Remark 2 The question remains how to determine the sample size over which the average should be taken. Qualitatively, the more variation is assumed in: (i) the network properties and (ii) the particle sizes, the larger the sample size should be. This is analogous to the fact that one needs a larger sample size to find the average of a wider random distribution than of a tighter one. However, it is unclear to us how to quantify the required sample size theoretically. Practically, however, one can do it by experimentation as follows. Start with a very narrow distribution of both the network properties and particle sizes. Verify that the above method and other methods, like the direct modeling of a thicker filter, do indeed produce the same result after averaging over some sample size. Then *gradually* (i.e., *by a little*) increase the variance in either the network properties or the particle size distribution. See if by increasing the sample size one can have the averages of the above and other methods coincide. If one indeed can, then proceed to further increase the variances. If not, an error somewhere needs to be found.

3 Implementation in a code and numerical results

3.1 Implementation details

Here we describe the implementation of a code that concatenates two single-filter codes, as restructured and annotated by Prof. Edwards in 2017. The single-layer codes are two-dimensional, as defined in the MPI 2009 report. This means that each filter is represented as a two-dimensional network, where one dimension (denoted as y in the code and below) corresponds to the direction of the liquid flux, while the other dimension (denoted as x) represents the random porous medium (*i.e.*, the filter) in the direction transverse to the flux. Recall that in those codes, flux through the filter is determined by the pressure drop δP (denoted as P in the code itself), the incidence matrix D, and pore sizes.

Denote the l-th single-layer[1] by a $x^l_{max} \times y^l_{max}$ network. For concatenated filters, we

[1]In the following we will (admittedly, somewhat sloppily) use words "layer" and "filter" to denote the

assume $y^l_{max} = y^1_{max}$ while $x^l_{max} = s^{l-1} \cdot x^1_{max}$. That is, the number of rows, $y_{\max}$, in each layer is the same and the number of columns in a given layer is s times that in the previous layer. Then we can calculate the incidence matrices, D^l, and assign pore sizes, d^l_i, to links between nodes in each single-layer network model. Here we consider a model with only two concatenated layers; thus $l = 1, 2$. One can generalize the two-layer model to multilayer models straightforwardly.

Once we get the essential parameters and matrices intialized for each layer, we can calculate the flux through them and start to run the clogging simulation of two-layer concatenation model using the following algorithm.

1. Calculate the pressure drop δP_l on each layer by Eq. (2); then calculate the probability distribution $P^l_{(k)(j)}$ that a particle travels directly from node (j) to node (k) along some edge k (defined in Section 3 of Prof. Edwards' report) in layer l.

   Consider a particle of diameter $d_{\rm P}$. Suppose that particles go through the layers one by one. The particle starts from the top layer, therefore we set $l = 1$.

2. The particle starts at the source, so set $(j) = (J^l - 1)$. Here (j) is the node where the particle is found in a given step and J^l is the total number of nodes in each layer. Thus, we order the nodes in a way that $(J^l - 1)$ is the source node; for the top layer in Fig. 1 it is depicted as the "bar" above the row of nodes. (Also, in the code, $(j) = J^l$ corresponds to the sink node, depicted in Fig. 1 by the single node in between the two layers.) Note that $J^l \equiv y^l_{\max} \cdot x^l_{\max} + 2$ may be different for each layer.

3. Choose a node (k) to which the particle will travel using the probability distribution $P^l_{(k)(j)}$. Then determine the edge number i as follows. Create a vector $\mathbf{v} \in \mathcal{R}^J$ with $v_{(j)} = -1$, $v_{(k)} = 1$, and all others entries being 0. Then when we compute the product $D\mathbf{v}$, the i-th element will have absolute value 2 (since both columns (j) and (k) will be nonzero in that row), and all the others will not.

4. If $d_{\rm P} \le d_i$, the particle passes through the pore.

   (a) If (k) is a sink node, defined in item 2 above, the particle has escaped the current layer.

      i. If $l = 2$, the particle has escaped the two-layer concatenated filter. Start a new particle simulation by setting $l = 1$: return to step #2.

      ii. Otherwise the particle is moving to the next layer; then set $l = l + 1$ and return to step #2

   (b) Otherwise set $(j) = (k)$ and go to step #3.

5. If $d_{\rm P} > d_i$, the particle clogs the pore represented by link i.

---

same thing.

(a) Set $d_i = 0$, which means from the definition of $P^l_{(k)(j)}$ that there will never be flow through edge i in layer l again.

(b) Given the new value of R^l, calculate p^l_i and $\mathbf{Q}^l$, where R^l and $\mathbf{Q}^l$ are the resistance matrix and the flux through each node, as defined in the 2009 MPI report.

(c) If $\mathbf{Q}^l \neq 0,\ l = 1, 2$, update the pressure drop $\delta P^l, l = 1, 2$ and the probabilities $P^l_{(k)(j)} l = 1, 2$ and then start simulating another particle as per step #2. Otherwise, the current layer is clogged, meaning the entire filter is clogged.

In our implementation of concatenation of two layers, there is no transition layer between them. Rather, the output of all pores in the last row of the first layer (located at the top in Fig. 1) is lumped to go into a single node (in the middle of Fig. 1). From there, the flow is distributed into the first row of the second layer.

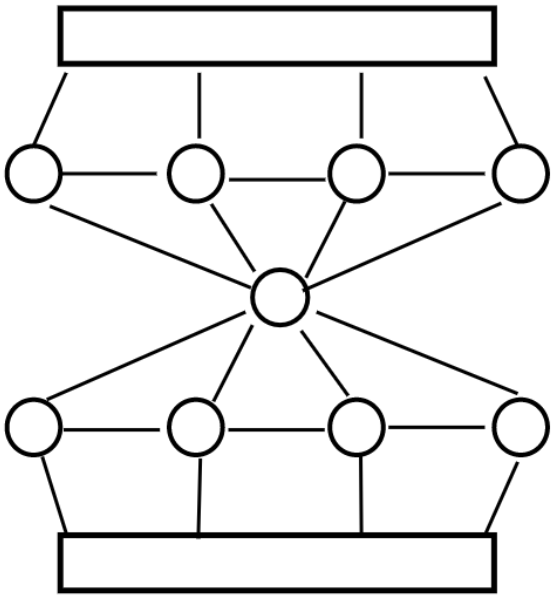

Figure 1: Schematics illustrating the two-layer concatenation model; here $y_{max} = 1, x_{max} = 4, s = 1$.

Remark 3 It should be noted that in the current implementation of the single-filter code, both the input and output links of your network can capture particles. In other words, the filter can get clogged both in its first layer of pores (links), which precedes the first row of nodes, and in the last row of pores (links), which follows the last row of nodes. This *should be modified* in later editions of the two-layer (and many-layer) code, because for the

concatenation idea to work, either only the input or only the output links, but *not both*, can capture particles.

3.2 Numerical results

In the following, we compare the behavior of our two-layer concatenation (global) model with the two-layer (local) model constructed by Prof. Edwards in 2017 and described in the previous chapter of this Report. The "global" model code is in twolayer.m and the "local" model code is in mlhc2d.m; each code can run independently of the other. Readers can see that many functions in them are named and organized similarly, which is because our "global" model code is build upon the "local" model code.

By the discussion in Prof. Edwards's section of this Report, the pore sizes d_i satisfy the gamma distribution, $d_i \sim \Gamma(k, \theta)$ with $k = 2, \theta = 0.0475$, implying that $\mathrm{E}[d_i] = k\theta$, $\mathrm{Var}[d_i] = k\theta^2$. For l-th layer, the pore size distribution is $d_i^l \sim \Gamma(k/s^{l-1}, \theta)$.

In the particle simulations, both codes use a random number generator in the process of predicting which pore the particle will move to. Therefore, in the simulations reported below, we ran the code 10 to 50 times and then took the average of the retention ratio and relative flux.

We run two different types of experiments (for two concatenated layers), distinguished by the scale parameter s.

- $s = 1$.

  In this case, the local model (developed by Prof. Edwards in 2017) is identical to the original one-layer network model of size $x^1_{max} \times 2 \cdot y^1_{max}$ (by our assumption of x^l_{max} and y^l_{max}, the sizes of the networks used to model both layers are the same). The pore size distribution is the same for both layers, and the connection between the nodes of the layers is one-to-one (each node in the lowest row of layer 1 is connected to one node in the top row of layer 2).

  On the other hand, our global model, illustrated by Fig. 1, can be viewed as two layers, with a middle node added between them. Otherwise, the parameters x_{max} and y_{max} and the pore size distribution are taken in our experiment to be the same as for the local model.

  1. First we test the case where all particles are of the same size, $d_\mathrm{P} = 0.05$. The retention ratio is expected to decrease to 0 and relative flux is expected to converge to a fixed value as discussed in the 2009 MPI report. We discovered a 0.8% difference in the averaged relative flux and a 2.9% difference in the averaged retention ratio between the two network models; see Fig. 2.

     It is unclear whether this difference is statistically significant, given the finite sampling size. However, assuming that it does represent the general trend, below we provide its explanation. Namely, the above comparison shows that more particles are retained in the global model than in the local model and a smaller relative

flux is observed in the global model. The possible reason for this phenomenon is that there are more pores (represented by links in edges in the network in Fig. 1) in the global model than in the local one due to the addition of another joint layer. This appears to be a plausible explanation since we observed (albeit more systematic studies are needed here) that the difference in the relative flux and retention ratio between the two models decreases as we increase the number of rows in a layer.

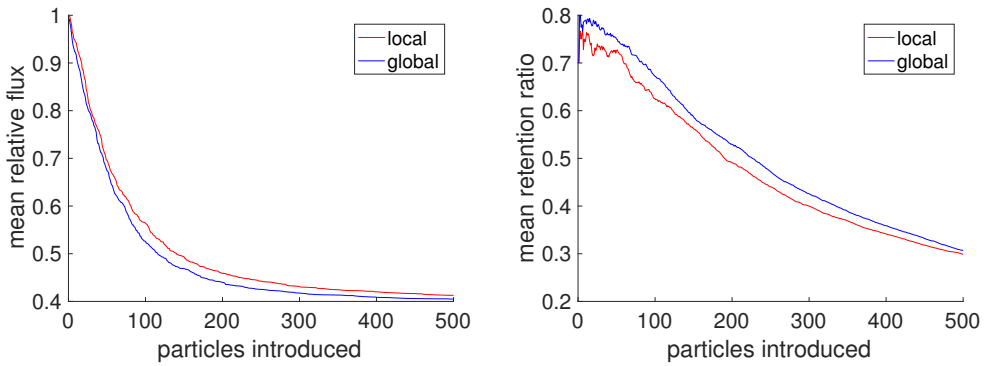

Figure 2: Comparison of local and global models for the average flux and retention ratio in 10 runs. Parameters: $s = 1$, particle diameter $d_{\mathrm{p}} = 0.05$, $x^1_{max} = 20$, $y^1_{max} = 40$.

2. Then we test the case $d_{\mathrm{P}} \sim \Gamma(k, \theta)$, where to the comparison pool of our two models — local and global — we have added the original single-layer network model described in the 2009 MPI report. As discussed there, the retention ratio is expected to increase to 1 and relative flux is expected to decrease to 0. We find (see Fig. 3) that the average relative flux looks similar for all three models, with a less than a 10% difference in the x-intercept, which indicates the number of particles needed to clog the whole filter. As for retention ratio, we see that the global and one-layer model both predict a significantly (by about 20%) smaller value of the lowest retention ratio. This means that the filter can capture more particles before being clogged according to the local model, described in this section of the report, than according to the global and single-layer models. This appears to be consistent with the other discrepancy betwen the two models, described at the end of the previous item.

3. Finally, we investigate the effect of increasing the variance of particle size distribution. To that end, we test the case $d_{\mathrm{P}} \sim \Gamma(k, 2\theta)$ and keep the pore size d_i distribution unchanged from the previous case. We see in Fig. 5 that as the variance is doubled (from θ to 2θ), the x-intercepts of two models are about the same. However, the discrepancy between the two models' prediction of the ratio

$$r_{\text{retention}} \equiv \frac{1 - \text{min retention ratio of local model}}{1 - \text{min retention ratio of global model}} \tag{4}$$

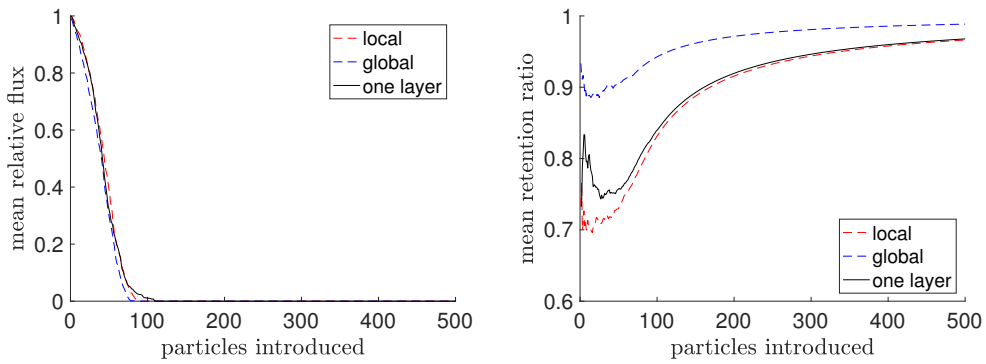

Figure 3: Comparison of the local, global, and original one-layer models for the average flux and retention ratio in 30 runs. Parameters: $s = 1$, particle diameter $d_\mathrm{p} \sim \Gamma(2, \theta)$, $x^1_{max} = 30$, $y^1_{max} = 10$. Note that the original one-layer model has $y_\mathrm{max} = 20$, *i.e.*, twice as many nodes as each layer in the two-layer models.

is greater for the greater variance. Specifically, from Fig. 5(b) this ratio can be estimated to be:

$$r_\mathrm{retention}(\theta) \sim r_\mathrm{retention}(2\theta) \sim 3 \ldots 4. \tag{5}$$

At present, the reason for this discrepancy between the two models is unclear and must be investigated further before one can advocate for a particular model, local or global. See also Remark 3 above.

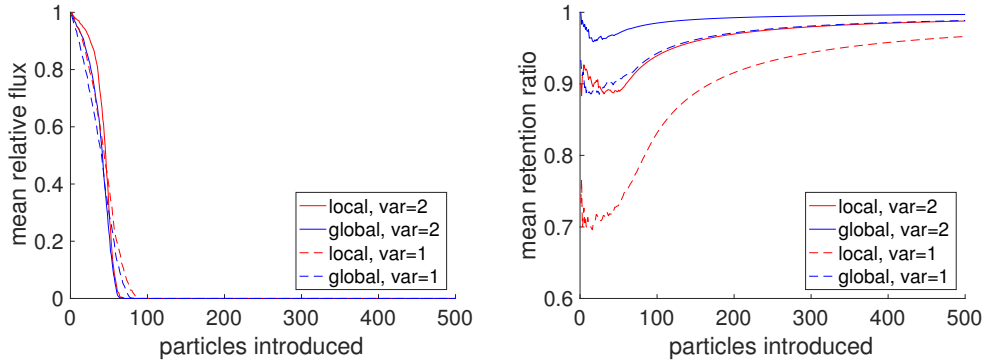

Figure 4: Comparison of local and global models for averaging flux and retention ratio in 30 runs for two models with $s = 1$, particle diameter $d_\mathrm{p} \sim \Gamma(2, 2 \cdot \theta)$. $x^1_{max} = 30$, $y^1_{max} = 10$.

- $s = 2$.

  In this case, the local and global models can be compared to one another but not to the original one-layer model, as the two layers now have different "densities" of nodes (and hence pores) per row. The pore size distribution is also allowed to be different in the two layers.

We test the cases $d_{\rm P} \sim \Gamma(\sqrt{2}, var\cdot\theta)$ for $var = 1, 2$. When $var = 1$, the x-intercepts of the relative flux also have a 10% difference as in the $s = 1$ case above. When $var = 2$, they are almost the same. As for the ratio (4), we found that

$$r_{\rm retention}(\theta) \approx \frac{0.28}{0.14} \approx 2; \qquad r_{\rm retention}(2\theta) \approx \frac{0.12}{0.03} \approx 4. \tag{6}$$

Thus, again, the global model predicts the retention of a greater share of particles. A relation of this discrepancy to the fact pointed out in Remark 3 remains to be investigated further.

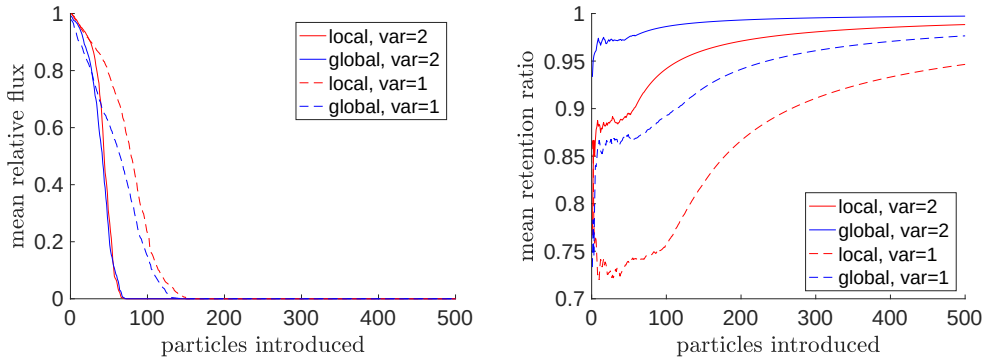

Figure 5: Comparison of local and global models for averaging flux and retention ratio in 30 runs for two models with $s = 2$, particle diameter $d_{\rm p} \sim \Gamma(\sqrt{2}, var\cdot\theta)$. $x^1_{max} = 30$, $y^1_{max} = 10$.

To summarize, both models, local and global, give close results for the number of particles needed to clog the filter. Also, that number decreases as θ, the variance of the pore size distribution, increases. On the other hand, the above preliminary results show a non-negligible discrepancy that may exist between the two models in predicting the retention ratio. It needs to be investigated further, perhaps following the guidelines in Remark 2 above.

4 Generalizations

Under the earlier assumption of the uniform redistribution of a filter's output into the input of the filter after it, the method described in Section 2 is generalized straightforwardly. For example, for 3 concatenated filters, one finds the pressure drops over each one of them from the system:

$$T_1(\delta P_1) - T_2(\delta P_2) = 0, \tag{7a}$$

$$T_2(\delta P_2) - T_3(\delta P_3) = 0, \tag{7b}$$

$$\delta P_1 + \delta P_2 + \delta P_3 = \delta P_{\rm tot}. \tag{7c}$$

The solution is given by the counterpart of (3):

$$\begin{pmatrix} \delta P_1^{(3)} \\ \delta P_2^{(3)} \\ \delta P_3^{(3)} \end{pmatrix} = \begin{pmatrix} \delta P_1^{(2)} \\ \delta P_2^{(2)} \\ \delta P_3^{(2)} \end{pmatrix} - J^{-1} \begin{pmatrix} T_1(\delta P_1^{(2)}) - T_2(\delta P_2^{(2)}) \\ T_2(\delta P_2^{(2)}) - T_3(\delta P_3^{(2)}) \\ \delta P_1^{(2)} + \delta P_2^{(2)} + \delta P_3^{(2)} \; - \; \delta P_{\rm tot} \end{pmatrix}, \tag{8a}$$

where the Jacobian

$$J = \begin{pmatrix} \frac{T_1(\delta P_1^{(2)}) - T_1(\delta P_1^{(1)})}{\delta P_1^{(2)} - \delta P_1^{(1)}} & -\frac{T_2(\delta P_2^{(2)}) - T_2(\delta P_2^{(1)})}{\delta P_2^{(2)} - \delta P_2^{(1)}} & \\ & \frac{T_2(\delta P_2^{(2)}) - T_2(\delta P_2^{(1)})}{\delta P_2^{(2)} - \delta P_2^{(1)}} & -\frac{T_3(\delta P_3^{(2)}) - T_3(\delta P_3^{(1)})}{\delta P_3^{(2)} - \delta P_3^{(1)}} \\ 1 & 1 & 1 \end{pmatrix}. \tag{8b}$$

Now let us point out how the distribution of a filter's output into the next filter's input can be made more "local". That is, how can we model the situation where the output of the left half of Filter 1 goes entirely into the input of the left half of Filter 2, and the output of the right half of Filter 1 goes entirely into the input of the right half of Filter 2? This can be done by an extension of the approach in Section 2. To describe that extension, consider again the case of just two filters. Then equations (2) get replaced with:

$$T_{1,i}(\delta P_{1,i}) - T_{2,i}(\delta P_{2,i}) = 0, \tag{9a}$$

$$\delta P_{1,i} + \delta P_{2,i} = \delta P_{\rm tot}; \tag{9b}$$

$$T_{1,ii}(\delta P_{1,ii}) - T_{2,ii}(\delta P_{2,ii}) = 0, \tag{9c}$$

$$\delta P_{1,ii} + \delta P_{2,ii} = \delta P_{\rm tot}. \tag{9d}$$

Here $\delta P_{j,i}$ ($\delta P_{j,ii}$), $j = 1, 2$ is the pressure drop over the left (right) half of Filter j, and $T_{j,i}(\delta P_{j,i})$ ($T_{j,ii}(\delta P_{j,ii})$) is the total flow through the left (right) half of each filter. Note that we have assumed that the output of the left half of Filter 1 enters *only* into the left half of Filter 2. We had to do so (or otherwise prescribe exactly what percentage of $T_{1,i}$ goes in to the left half for Filter 2) since the problem would have been under-determined otherwise.

System (9) can also be solved by the secant method. However, unlike the cases considered earlier, here $T_{j,i}$ and $T_{j,ii}$ are *not* linear functions of their respective pressure drops, because the halves of the filter are connected. Consequently, the generalization of Eqs. (3) will provide the next iteration towards the exact solution, but not the solution itself, of (9). However, in practice, the secant method converges fast, and this issue is not expected to slow down the algorithm considerably (maybe, it will slow it down by a factor of two or so).

The extension of the above idea to the case where each filter is subdivided into M parts is straightforward. Thus, concatenating N filters, each of which is subdivided into M parts, will require the solution of a system of NM equations by the secant method.

Porous Media: Continuous Model

C. Breward, J. Chapman
Oxford University

L. Cummings
New Jersey Institute of Technology

D. A. Edwards
University of Delaware

T. Phan
Arizona State University

1 Governing Equations

We consider a continuous model of the filtration of particles of n different sizes through a porous medium. We consider a one-dimensional transport model:

$$\frac{\partial(\epsilon\tilde{C}_i)}{\partial\tilde{t}} + \frac{\partial}{\partial\tilde{x}}\left(\tilde{U}\tilde{C}_i\right) = D_i\frac{\partial^2\tilde{C}_i}{\partial\tilde{x}^2} - \tilde{S}_i, \qquad i = 1, 2, \ldots, n. \tag{1}$$

Here $\tilde{C}_i$ is the concentration of the particle of size i in the underlying fluid, ϵ is the porosity of the medium, $\tilde{U}$ is the Darcy velocity, and D_i is the molecular diffusion coefficient for the particle of size i. The sink term $\tilde{S}_i > 0$ represents adsorption of the particles to the sides of the pores. This adsorption process also clogs the pore, and so the porosity decreases proportionally to each of the adsorption processes:

$$\frac{\partial\epsilon}{\partial\tilde{t}} = -\sum_{i=1}^{n}\alpha_i\tilde{S}_i, \tag{2}$$

where α is a proportionality constant. (For more details on the derivation of (1), see [1, §3.2].)

We simplify our model by assuming that all the particles are of one size (so we drop the

subscript i from $\tilde{C}$). Furthermore, by computing the Péclet number for the system (which measures the ratio of convective effects to diffusive ones), we obtain a value which is higher than 10^3. Hence we can assume the diffusion term does not contribute much in the process, so we neglect the diffusion term in (1). This makes physical sense, as the fluid is assumed to be pushed through the filter so the advection term is significantly larger than diffusion term. Hence our system (1) and (2) reduces to

$$\begin{aligned} \frac{\partial(\epsilon\tilde{C})}{\partial\tilde{t}} + \tilde{U}\frac{\partial\tilde{C}}{\partial x} &= -\tilde{S}, \\ \frac{\partial\epsilon}{\partial\tilde{t}} &= -\alpha\tilde{S}. \end{aligned} \tag{3}$$

Phenomenologically, the rate of clogging increases with higher concentration, so for simplicity, take

$$\tilde{S} = \lambda\tilde{C}, \tag{4}$$

where λ is a constant measuring how likely a particle is to stick to the side of the pore [2, §2.3]. This constitutive relation is motivated by models of electrostatic attraction. Thus our system (3) reduces to

$$\frac{\partial(\epsilon\tilde{C})}{\partial\tilde{t}} + \tilde{U}\frac{\partial\tilde{C}}{\partial\tilde{x}} = -\lambda\tilde{C}, \tag{5}$$

$$\frac{\partial\epsilon}{\partial\tilde{t}} = -\alpha\lambda\tilde{C}. \tag{6}$$

We assume the fluid is incompressible, which means the spatial derivative of the flow velocity is negligible. Hence we take

$$\frac{\partial\tilde{U}}{\partial\tilde{x}} = 0. \tag{7}$$

$\tilde{U}$ can be obtained from the pressure gradient *via* Darcy's Law [1, §1.4.1]:

$$\tilde{U}(\tilde{t}) = -\frac{k}{\mu}\frac{\partial\tilde{P}}{\partial\tilde{x}}, \tag{8}$$

where $\tilde{P}$ is the pressure and μ is the viscosity of the fluid. The intrinsic permeability k of the medium depends on the porosity according to the Kozeny-Carmen equation

$$k(\epsilon) = \frac{\chi\epsilon^3}{(1-\epsilon)^2}, \tag{9}$$

where χ represents the local structure of the porous material. Moreover, we have used (7) to write $\tilde{U}$ as a function solely of $\tilde{t}$.

The filter occupies the region $\tilde{x} \in [0, h]$. At the top of the filter ($\tilde{x} = h$), the concentration is a given constant:

$$\tilde{C}(h, \tilde{t}) = C_*, \tag{10}$$

while at the bottom of the filter, the pressure is assumed to be 0:

$$\tilde{P}(0, \tilde{t}) = 0. \tag{11}$$

Initially, the porosity in the medium is known, and the concentration is 0:

$$\epsilon(\tilde{x}, 0) = \epsilon_*(\tilde{x}), \qquad \tilde{C}(\tilde{x}, 0) = 0. \tag{12}$$

1.1 Scaling

To simplify the problem for further analysis, we scale our variables. Motivated by (10), we let

$$C(x, t) = \frac{\tilde{C}(\tilde{x}, \tilde{t})}{C_*}, \qquad x = \frac{\tilde{x}}{h}. \tag{13}$$

There are several time scales in the problem. As we are most interested in the process by which the filter clogs, we choose a time scale which balances the porosity evolution equation (6). Substituting (13) into (6), we obtain

$$\begin{aligned} \frac{\partial \epsilon}{\partial \tilde{t}} &= -\alpha \lambda C_* C \\ \frac{\partial \epsilon}{\partial t} &= -C, \qquad t = \alpha \lambda C_* \tilde{t}. \end{aligned} \tag{14}$$

In a typical experiment, the pressure at the top of the filter may be kept at a constant value P_*, so we have

$$P(x, t) = \frac{\tilde{P}(\tilde{x}, \tilde{t})}{P_*}. \tag{15}$$

Substituting (13) and (15) into (8) yields a scaling for $\tilde{U}$:

$$\tilde{U}(\tilde{t}) = -\frac{P_*}{h\mu} \frac{\partial P}{\partial x} \frac{\chi \epsilon^3}{(1-\epsilon)^2}$$

parameter	value	unit	source
C_*	10^{-3}	$\mathrm{mol/m^3}$	Gore
h	10^{-4}	m	Gore
pore radius	2.5×10^{-8}	m	Gore
ϵ_*	0.1 - 1	unitless	Gore
λ	0.1	$\mathrm{s^{-1}}$	guess
μ	10^{-3}	$\mathrm{N \cdot s/m^2}$	Gore
χ	10^{-16}	$\mathrm{m^2}$	Gore

Table 1: Table of parameter values.

$$U(t) = -\frac{\epsilon^3}{(1-\epsilon)^2}\frac{\partial P}{\partial x}, \qquad U(t) = \frac{\tilde{U}(\tilde{t})h\mu}{P_*\chi}. \tag{16}$$

Substituting the scales in (13), (14), and (16) into (5), we obtain

$$\begin{aligned} C_*(\alpha\lambda C_*)\frac{\partial(\epsilon C)}{\partial t} + \frac{P_*\chi C_*}{h^2\mu}U\frac{\partial C}{\partial x} &= -\lambda C_* C, \\ L_{\mathrm{C}}\frac{\partial(\epsilon C)}{\partial t} + U\frac{\partial C}{\partial x} &= -C_{\mathrm{B}} C, \qquad (17) \\ C_{\mathrm{B}} = \frac{\lambda\mu h^2}{P_*\chi}, \qquad L_{\mathrm{C}} &= \frac{\alpha\lambda C_* h^2\mu}{P_*\chi} = \alpha C_* C_{\mathrm{B}}. \qquad (18) \end{aligned}$$

Estimated values of the experimental parameters are summarized in Table 1. With these values, one may compute other parameters. In particular, assuming a spherical shape for the pore, we have that the pore volume is given by

$$\frac{4}{3}\pi(2.5)^3 \times 10^{-24}\ \mathrm{m^3} \approx 5 \times 10^{-23}\ \mathrm{m^3}.$$

Then noting that α must have units of inverse concentration, and is related to the concentration (in molecules) near the surface of the pore, we use Avogadro's number to compute

$$\alpha \approx 5 \times 10^{-23}\ \mathrm{m^3} \cdot \frac{6 \times 10^{23}}{\mathrm{mol}} = 30\frac{\mathrm{m^3}}{\mathrm{mol}}. \tag{19}$$

With this value in hand, we can compute our two dimensionless ratios:

$$C_{\mathrm{B}} = \frac{\lambda\mu h^2}{P_*\chi} \approx \frac{(10^{-1})(10^{-3})(10^{-8})}{(10^5)(10^{-16})} = 10^{-1},$$

$$L_{\mathrm{C}} = \alpha C_* C_{\mathrm{B}} \approx (30)(10^{-3})(10^{-1}) \approx 10^{-3},$$

We treat C_{B} as $O(1)$, but L_{C} as $o(1)$, so we may neglect the first term in (17), yielding

$$U\frac{\partial C}{\partial x} = -C_{\mathrm{B}} C, \tag{20}$$

so we are in the steady state of the evolution equation. Hence we ignore the initial condition for $\tilde{C}$ in (12). Hence the important boundary and initial conditions are given by

$$C(1,t) = 1, \qquad \epsilon(x,0) = \epsilon_*(x), \tag{21}$$

$$P(0,t) = 0. \tag{22}$$

Solving (20) subject to (21), we have

$$C(x) = e^{-w(t)(1-x)}, \qquad w(t) = -\frac{C_{\mathrm{B}}}{U(t)} > 0. \tag{23}$$

1.2 Relating the Pressure and Velocity

We may manipulate and integrate (16) to obtain the following relationship between the pressure and velocity:

$$\begin{aligned} \frac{\partial P}{\partial x} &= -\frac{(1-\epsilon)^2}{\epsilon^3} U(t) \\ P &= -U(t) \int_0^x \frac{(1-\epsilon(s,t))^2}{\epsilon(s,t)^3}\, ds, \end{aligned}$$

where we have used (22). The other place where the pressure is known is at the top of the filter, where we have

$$P(1,t) \equiv P_1(t) = -I(t)U(t), \qquad I(t) = \int_0^1 \frac{(1-\epsilon)^2}{\epsilon^3}\, dx. \tag{24}$$

Recall that with the orientation of x, $U < 0$.

Hence our final system is given by (14), (20), and (24), subject to (21).

2 Constant Flux

In practice, there are two ways to implement this system. The first is to maintain a constant flux (and hence U) at $x = 1$; the other is to keep a constant pressure there. If U is constant, then w is constant. Substituting (23) with w constant into (14) and integrating, we have

$$\epsilon(x,t) = \epsilon_*(x) - e^{-w(1-x)}t, \tag{25}$$

where we have used (21). Therefore, we see that as t increases, there will be some time t_0 for which $\epsilon(x,t_0) = 0$ for some x. At that point, the filter is clogged. Also note from (24), as $\epsilon \to 0$, $I \to \infty$ and hence the pressure needed to maintain the constant flux grows without bound.

2.1 Constant Initial Porosity

If the initial porosity is set at a constant ϵ_0, then (25) becomes

$$\epsilon(x,t) = \epsilon_0 - e^{-w(1-x)}t.$$

The largest negative contribution comes from $x = 1$, and hence we have that

$$\min_x \epsilon(x,t) = \epsilon(0,t) = \epsilon_0 - t,$$

from which we have that $t_0 = \epsilon_0$, and the filter clogs at the top. This is the behavior seen experimentally.

2.2 Exponential Initial Porosity

Motivated by the form of (25), we consider the case where the initial porosity matches the concentration profile:

$$\epsilon_*(x) = \gamma e^{-w(1-x)}, \tag{26}$$

where $\gamma > 0$ is some constant. Such an initial profile is consistent with layered filters currently used (see Fig. 2.2).

Substituting (26) into (25), we obtain

$$\epsilon(x,t) = e^{-w(1-x)}(\gamma - t),$$

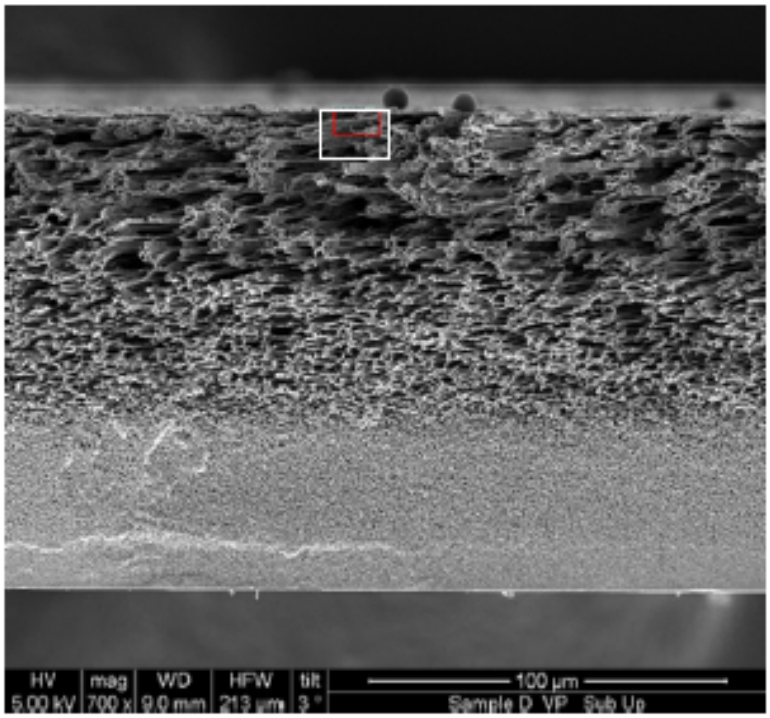

Figure 1: Picture of layered filter [3]. Here the particles enter at the top, and exit at the bottom. Note the variation in pore size from top to bottom, as well as the large particles adhering to the top.

where $\gamma > 0$ is some constant. In this case the porosity decreases proportionally all along the length of the porous media. As a result, when the filter clogs at $t_0 = \gamma$, it does so because $\epsilon = 0$ for all x. This would seem to be the ideal design for a filter, because no empty voids are wasted because of a clog upstream.

2.3 Comparing the Profiles

In order to make a more quantitative comparison, we consider two filters (made of the same material) to be *comparable* if the pressure needed to drive pure liquid through both is identical. In other words, given U, $P_1(0)$ is the same for both filters, which from (24) just means that $I(0)$ is the same for both filters.

Given two comparable filters, we say that one is *preferable* if it has a larger total amount of particles absorbed by the time the filter fails. Hence we integrate our sink term $\tilde{S}$ over all

space and time; in our dimensionless context, that means we compute

$$J \equiv \int_0^{t_0} \int_0^1 C(x,t)\,dx. \tag{27}$$

In our case, we have

$$J = t_0 \left[\frac{e^{-w(1-x)}}{w}\right]_0^1 = \frac{t_0(1-e^{-w})}{w},$$

where we have used (23), and hence a filter is preferable if its failure time is larger.

Making the two types of filters comparable provides a condition on γ and ϵ_0:

$$\int_0^1 \frac{(1-\epsilon_0)^2}{\epsilon_0^3}\,dx = \int_0^1 \frac{(1-\gamma e^{-w(1-x)})^2}{\gamma^3 e^{-3w(1-x)}}\,dx.$$

However, we have that $\gamma e^{-w(1-x)} < \gamma$ except at $x = 0$. Hence the numerator of the integrand is smaller if we remove the exponential, and the denominator is smaller. Hence we have

$$\frac{(1-\epsilon_0)^2}{\epsilon_0^3} > \int_0^1 \frac{(1-\gamma)^2}{\gamma^3}\,dx = \frac{(1-\gamma)^2}{\gamma^3}, \tag{28}$$

where we have used the fact that ϵ_0 and γ are both constants in $[0,1]$. But by the arguments we used before, we see that (28) will be satisfied if $\epsilon_0 < \gamma$, since then the numerator on the left is larger than its counterpart on the right, and the denominator on the left is smaller than on the right. Hence $\epsilon_0 < \gamma$, which means that the failure time for the exponential porosity is longer, which makes it a better filter.

3 Constant Pressure

Now suppose that we keep P_1 constant instead, which we take to be $P_1 = 1$ without loss of generality. Then from (24) we have

$$-\frac{1}{U(t)} = \frac{I(t)}{P_1(t)} \qquad \Longrightarrow \qquad w(t) = C_{\mathrm{B}} I(t).$$

Hence it follows from (14) that

$$\frac{\partial \epsilon}{\partial t} = -e^{-w(t)(1-x)},$$

which cannot be easily integrated. Therefore, we see that if we can reduce the Breward constant while keeping the Linda constant small, the porosity will decay at a slower rate. However, from (18) we can see that this can be done only by decreasing either α or C_* while increasing C_{B}.

4 More Complicated Sink Terms

4.1 New Equations

Note from (14) that

$$\frac{d\epsilon(1,t)}{dt} = -C(1,t) = -1$$

for any experiment. Hence the porosity decays linearly at the top of the filter, which seems unsatisfactory. Therefore, we propose more realistic sink terms.

For simplicity, consider a pore with a circular cross section. First, we note that if we consider attraction to the walls, the rate at which the particles adhere should be proportional to how many molecules are within some distance dr from the wall. And as those particles adhere, they will reduce the cross-sectional area A. Hence we have that

$$\frac{dA}{dt} \propto 2\pi r\, dr,$$

where the right-hand side is the area of a thin shell near the wall. If we consider a spherical pore of volume V, we have

$$\frac{d(V^{2/3})}{dt} \propto V^{1/3},$$

where we treat dr as a constant. But the porosity is proportional to the volume of the pores, so we have

$$\frac{2}{3\epsilon^{1/3}}\frac{d\epsilon}{dt} \propto \epsilon^{1/3}$$
$$\frac{d\epsilon}{dt} \propto \epsilon^{2/3},$$

so we could replace (4) with

$$\tilde{S} = \lambda \tilde{C} \epsilon^{2/3}. \tag{29}$$

However, there is also a mechanism by which particles can block smaller pores entirely.

That process is not only proportional to $\tilde{C}$, but also to $\tilde{U}$, since the faster the flow rate, the more molecules can reach pores which it is possible for them to block. Hence we would have a sink term of the form

$$\delta \tilde{U} \tilde{C} f(\epsilon),$$

where δ is a proportionality constant (perhaps based on the pore geometry or structure) and $f(\epsilon)$ is a dimensionless function of ϵ. When the porosity is 1, the pores are so large that they can't be blocked, so $f(0) = 0$. As the porosity tends to zero, the pores are so small that they can be easily blocked, so the sink term saturates and $f(1) = 1$.

The easiest function to use would be a linear one. Since the blocking mechanism is dictated by the relative size of the radii of pore and particle, f should really depend on r, which is proportional to $\epsilon^{1/3}$. Hence we could replace (4) with

$$\tilde{S} = \lambda \tilde{C} \epsilon^{2/3} + \delta \tilde{U} \tilde{C} (1 - \epsilon^{1/3}) \tag{30}$$

to take into account both mechanisms. Making these replacements, (5) and (6) become

$$\frac{\partial(\epsilon \tilde{C})}{\partial \tilde{t}} + \tilde{U} \frac{\partial \tilde{C}}{\partial \tilde{x}} = -\left[\lambda \tilde{C} \epsilon^{2/3} + \delta \tilde{U} \tilde{C} (1 - \epsilon^{1/3})\right], \tag{31}$$

$$\frac{\partial \epsilon}{\partial \tilde{t}} = -\alpha \left[\lambda \tilde{C} \epsilon^{2/3} + \delta \tilde{U} \tilde{C} (1 - \epsilon^{1/3})\right]. \tag{32}$$

4.2 Numerical Results

Equation (31) and (32) are difficult to solve analytically; thus we provide numerical results instead. We provide the numerical simulation for the constant flux case with parameters in Tab. 1.

In Fig. 2, we consider the case where the initial porosity profile $\epsilon(x)$ is constant. This would correspond to a filter made of a single layer of material. Note that as time proceeds, the porosity decreases most at the inlet end $x = 1$, as expected. Also, the concentration changes most at the inlet end, reinforcing that most of the filtration is occurring at the inlet. Not very many particles are reaching the downstream end, which is why the porosity doesn't change very much there.

In Fig. 3, we model the case where the initial porosity profile $\epsilon(x)$ varies in a piecewise-constant fashion. This models a filter consisting of a series of layers. Note from the left figure in Fig. 3 that the porosity increases as x increases, corresponding to the finest filter at the outlet, and the coarsest filter at the inlet.

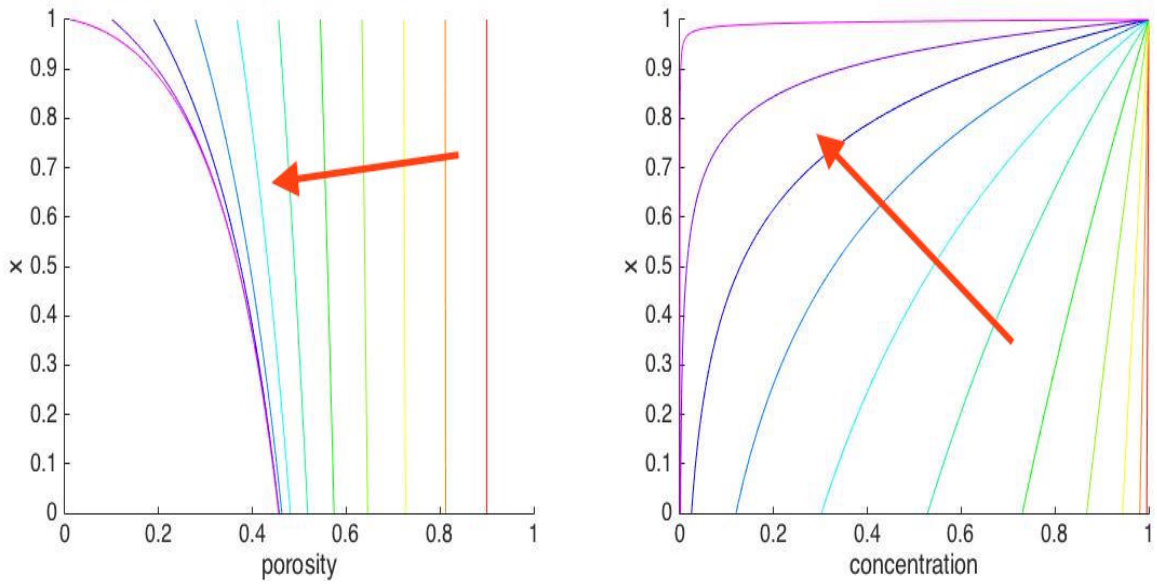

Figure 2: The case of constant initial profile of porosity. The red curve represents the initial condition; while the red arrow represents the evolution with respect to time. The initial porosity of the filter is assumed to be homogeneous in space.

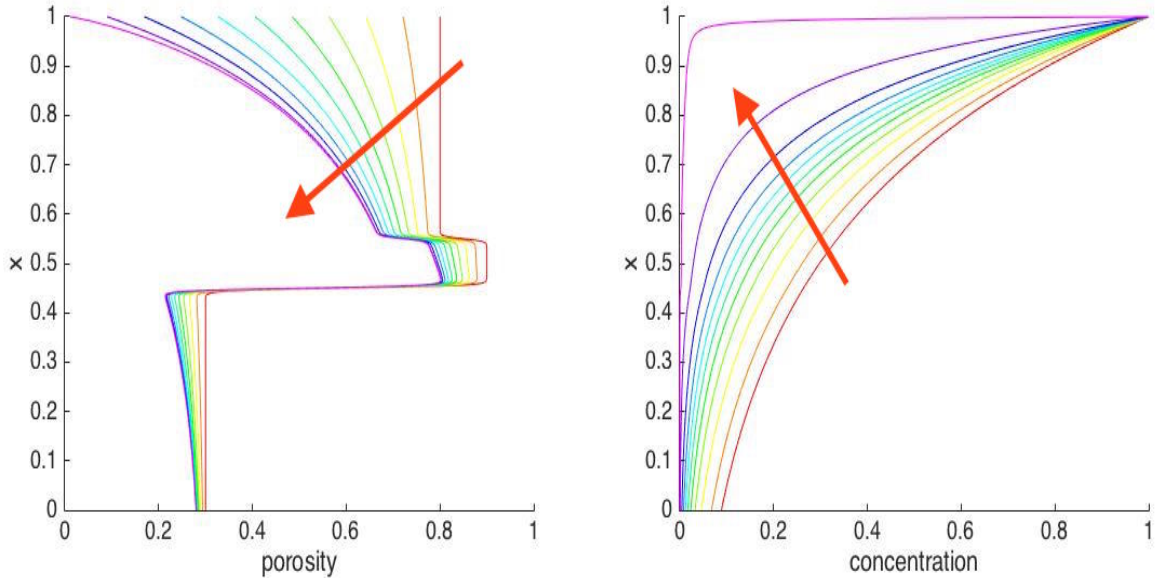

Figure 3: The case of non-constant initial profile of porosity. The red curve represents the initial profile; while the red arrow represents the evolution with respect to time. The variation in the initial porosity profile represents the two different layers with a connecting dip.

Note that as time proceeds, the porosity decreases most at the high end *of each layer*; in other words, each layer behaves like the constant-profile case in Fig. 2. Even though the porosity is largest in the topmost filter, the porosity decreases the most there, eventually clogging the filter. This is reasonable, as the top layer still filters the most particles, given its large porosity. Hence the concentration of particles in the flow decreases significantly before reaching the next layer, as shown in Fig. 3. Also, note that the concentration profile is smooth because a smooth transition is used to connect the discontinuities in our numerical work.

5 Conclusions

In this chapter we proposed a continuous model for the filtration of particles in a porous media. Given the large Péclet number for the filter, diffusion can be neglected and the full system (1) and (2) can be reduced to (3). Given the simple form (4) for the adsorption term, the problem simplifies further to (14) and (20) with appropriate scalings. Using Darcy's Law, we established the relationship (24) between the pressure at the inlet and the velocity in the filter.

In the case of constant flux, the problem admits analytical solutions for the concentration C and the porosity ϵ. These demonstrate that the blocking process is fastest at the inlet, causing a pore with constant initial ϵ to block at $x = 1$. The multi-layer filters we wish to describe can be approximated with an exponentially varying porosity. We showed that such a porosity profile leads to a longer failure time, and hence a better filter.

In the more realistic case of constant inlet pressure, solutions must be generated numerically. We also introduced a more complicated expression (30) for the particle sink at the pores. Numerical simulations of the resulting equations again demonstrated that the pores tend to clog at the upstream end, no matter the underlying porosity.

Nomenclature

Units are listed in terms of mass (M), moles (N), length (L), time (T), and temperature (θ). If a symbol appears both with and without tildes, the symbol with tildes has units, while the one without is dimensionless. Equation numbers where a variable is first defined is listed, if appropriate.

A: characteristic cross-sectional area of pore.

$\tilde{C}$: concentration of particles, units N/L^3 (1).

C_{B}: dimensionless constant multiplying sink term in (17).

D: diffusion coefficient, units L^2/T (1).

$f(\epsilon)$: sink term characterizing blocking.

h: height of filter, units L (10).

I: integral relating velocity to pressure (24).

i: indexing variable (1).

J: measure of accumulated flux (27).

k: intrinsic permeability, units L^2 (8).

L_{C}: dimensionless constant multiplying evolution term in (17).

$\tilde{p}$: pressure, units $M/(LT^2)$ (8).

r: characteristic radius of pore.

$\tilde{S}$: particle sink term, units N/L^3T (1).

$\tilde{t}$: time, units T (1).

$\tilde{U}$: Darcy velocity, units L/T (1).

V: characteristic volume of pore.

$w(t)$: exponent in expression for C (23).

$\tilde{x}$: distance from inlet, units L (1).

α: proportionality constant in porosity evolution equation (2), units L^3/N.

γ: constant in exponential initial profile for ϵ (26).

δ: constant in blocking sink term, units L^{-1}.

ϵ: porosity (1).

λ: proportionality constant in sink equation (4), units T^{-1}.

μ: viscosity of fluid, units $M/(LT)$ (8).

χ: proportionality constant in Kozeny-Carmen equation (9), units L^2.

Other Notation

$i \in \mathcal{Z}$: as a subscript on $\tilde{C}$, used to indicate a particle size (1).

0: as a subscript on ϵ, refers to a constant initial value; as a subscript on t, refers to fouling time.

1: as a subscript on P, refers to the value at $x = 1$ (24).

$*$: as a subscript on C, used to indicate a characteristic value (10); as a subscript on ϵ, used to indicate an initial condition (12).

References

[1] D. Nield and A. Bejan, *Convection in Porous Media*. New York: Springer, 2006.

[2] F. Civan, *Porous Media Transport Phenomena*. Hoboken: Wiley, 2011.

[3] W. Li, *Fouling Models for Optimizing Asymmetry of Microfiltration Membranes*. Cincinnati: University of Cincinnati, 2009.

Study of dependence of a double-layer filter performance on depths of filter's layers

Ryan Allaire
NJIT

Marina Chugunova
Claremont Graduate University

Taras Lakoba
University of Vermont

All our numerical simulations are based on the model derived for a one-layer filter by Faruk Civan in [1].

Consider a porous medium whose initial and instantaneous effective (interconnected) porosities are denoted by ϕ_i and ϕ. Let u and ρ represent the volumetric flux and density of the flowing fluid containing fine particles. ρ_p is the particle material mass density. w and σ denote the mass and volume fractions of particles present in the flowing fluid medium. ε is the volume fraction of particles deposited in bulk porous media. t and x denote the time and distance from the injection point.

Consider a one-dimensional model of a filter (porous media material) with $x \in [0, L]$. The time evolution of the volume fraction of particles deposited in porous media can be calculated as follows

$$\frac{\partial \varepsilon}{\partial t} = \kappa\, u\, (\sigma - d \cdot \nabla \sigma)\,, \tag{1}$$

where $\varepsilon = 1 - \phi$ and $\varepsilon = 1 - \phi_i$ at $t = 0$. Here $\sigma = \sigma(x, t)$ represents the volume fraction of particles in the flow. Furthermore, $d = \alpha\tau$, where α is the longitudinal dispersion of the filter, and τ is the tortuosity of the filter.

Let A_h, P_h, L_h denote the cross-sectional area, perimeter, and length of the mean hydraulic flow tube. n denotes the number of hydraulic tubes providing flow through the porous media. Then, the bulk volume of porous medium and the pore volume of all the hydraulic tubes V_p in a bulk representative elementary volume V_b of porous media are given respectively by $V_b = A_b\, L_b$, $V_p = n\, A_b\, L_b$.

The tortuosity τ of the mean hydraulic tube is defined as the ratio of the hydraulic tube length L_h to the bulk length L_b, so $\tau = L_h/L_b$.

We consider Darcy Flow, enabling us to write

$$u = -\frac{K}{\mu}\left(\frac{\partial P}{\partial x} - \rho g\right) \tag{2}$$

where

$$K = \phi^{2\nu+1}\,\gamma^2\,\left(\frac{\phi}{1-\phi}\right)^{2\,\beta}.$$

The coefficients ν, γ, and β are given by

$$\beta = \frac{1}{2(1 - D_1/\widetilde{D_1})},$$

$$\nu = \frac{1}{2}\left(\frac{d_1}{3} - 1\right),$$

$$\gamma = \frac{\exp\left[\ln n\,(3 - D_1)(2/(\widetilde{D_1} - D_1))\,(C_1/\widetilde{C_1})^{\frac{3}{(2(\widetilde{D_1} - D_1))}}\right]}{2\tau\sqrt{2\pi L_b/C_1}}.$$

The cross-sectional area open for flow, the areosity of porous media, is given by a fractional relation: $A_b\,\tilde{c_1}\phi^{\tilde{d_1}/3} = nA_h$ that determines $\tilde{d_1}$ and $\tilde{c_1}$ implicitly.

The total pore surface $n\,P_h\,L_h = \widetilde{C_1}[V_b\Sigma_b]^{\widetilde{D_1}/3}$ (Σ_b is a total pore surface per unit bulk volume) that determines $\widetilde{D_1}$ and $\widetilde{C_1}$, also implicitly.

Scaling parameters c_1, d_1, C_1, D_1 are empirical values, found by fitting to experimental data.

This form generalizes a well-known Kozeny–Carman relation ($\beta = 1$ case):

$$K = \delta^2\,\frac{\phi^3}{180(1-\phi)^2},$$

where δ is an average size of grains in porous media.

The limitation of the Kozeny–Carman model is due to the assumption that the flow tubes remain open or conductive at all times because of the definition of hydraulic tubes and the use of this concept for realization of porous media. Therefore, this model is primarily intended for applications to static porous materials, whose effective or conductive pore structure and properties (porosity, permeability, tortuosity, and so on) remain unchanged during fluid flow (cf. [2]).

The parameter μ is the dynamic viscosity of the fluid. σ here is governed by conservation of mass:

$$\begin{aligned}
&\frac{\partial\sigma}{\partial t} + a\frac{\partial\sigma}{\partial x} + b\sigma = c\frac{\partial^2\sigma}{\partial x^2},\\
&a = \frac{u}{\phi}\left(1 - \left[1 - \frac{\rho_P}{\rho}\sigma\right]\kappa d\right),\\
&b = \frac{u}{\phi}\left[1 - \frac{\rho_P}{\rho}\sigma\right]\kappa,\\
&c = \frac{u}{\phi}d,\\
&\sigma(x,0) = \sigma_0(x).
\end{aligned}$$

In our computations we will neglect the diffusion term because of the large value of the Péclet number: $\sim 10^3$. Thus, all terms proportional to d in the above equations are set to zero. Moreover, we also neglect the term proportional to σ with coefficient b, because $\sigma \sim 10^{-4}$ and $\rho_P/\rho \approx 1$.

For numerical simulations (via a finite difference scheme implemented in Matlab) the following numeric values for the parameters in the above equations were used:

$$\phi(t=0) = 0.8\ldots0.9; \qquad \kappa = 10^5\ldots10^6\,\mathrm{m}^{-1}; \qquad \mu = 10^{-3}\,\mathrm{Pa}\cdot\mathrm{s},$$

$$\chi = 10^{-16}\,\mathrm{m}^2; \qquad h = 10^{-4}\,\mathrm{m}; \qquad P = 10^5\,\mathrm{Pa}. \tag{3}$$

Figure 1 illustrates that after a short period of time (approximately 0.02 seconds) the concentration of particles stabilizes.

Figure 2 illustrates the main disadvantage of a uniform one-layer filter. Namely, most of the clogging occurs near the top of the filter and thus most of filter's material is left unused at the time when the top of the filter gets completely clogged. This results in a short lifetime of the filter. One of solutions which can make a filter's clogging more uniform through the depth of the filter is construction of multi-layer filters.

Figure 3 shows results of simulations for a two-layer filter for different values of its layers' depths (the top layer has pore diameter 4 times larger than the bottom one). The blue line corresponds to the 50/50 case, where both layers have the same depth. The red line corresponds to the 70/30 case, where the coarse filter takes 70 percent of the total depth, and the green line corresponds to the 30/70 case, where the coarse filter takes only 30 percent of the total depth. If we, for the moment, define the best-performing filter as that yielding the maximum total (*i.e.*, integrated over time) flow of the filtrate, then the best performance is exhibited by the 70/30 filter (red line).

Thus, for the simple model that we used, it is obvious that for the case of two-layer filtration, the fine filter should have the smallest depth (which is constrained only by its ability to reduce the original concentration of particles to a prescribed, near-zero value).

The above analysis can be straightforwardly extended to optimize a multi-layer filter. Namely, we first define a quantity that needs to be optimized. Instead of the total filtrate

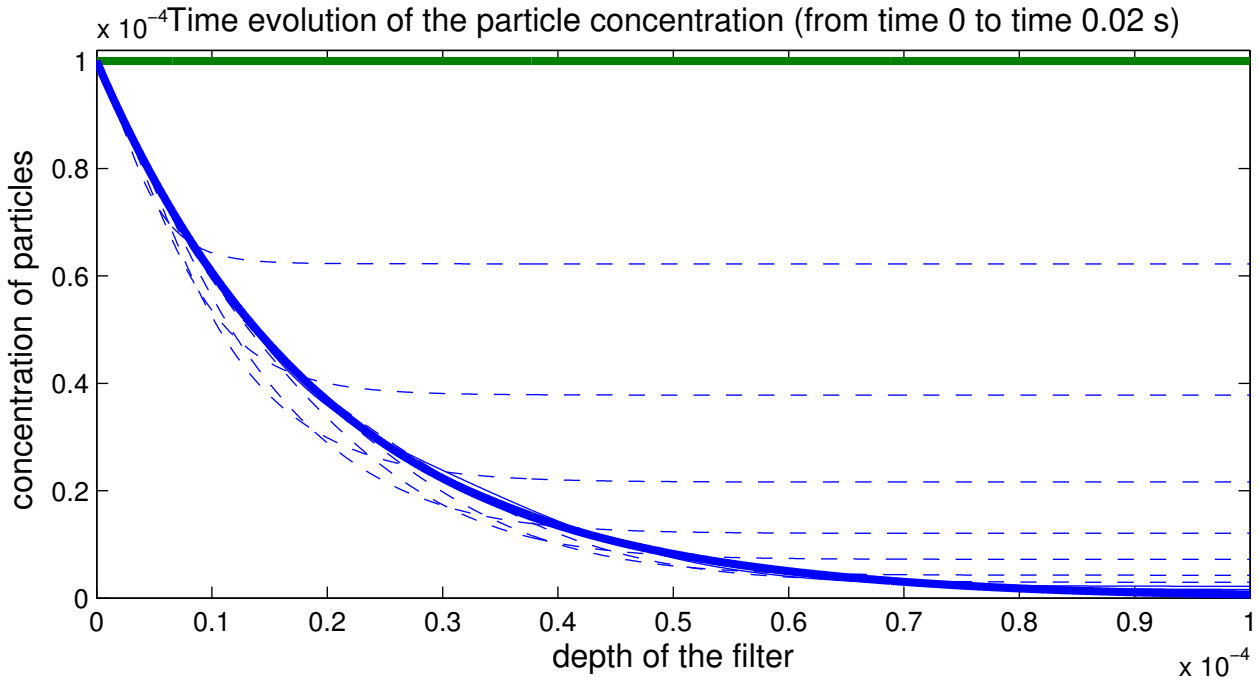

Figure 1: Illustration of particle concentration stabilization for the continuous model. Time snapshots of particle concentration for time $t < 0.02$ s are shown by dashed lines; the decreasing values of $\sigma(x = h, t)$ in the plot correspond to increasing values of t. The solid line is for $t = 0.02$ s.

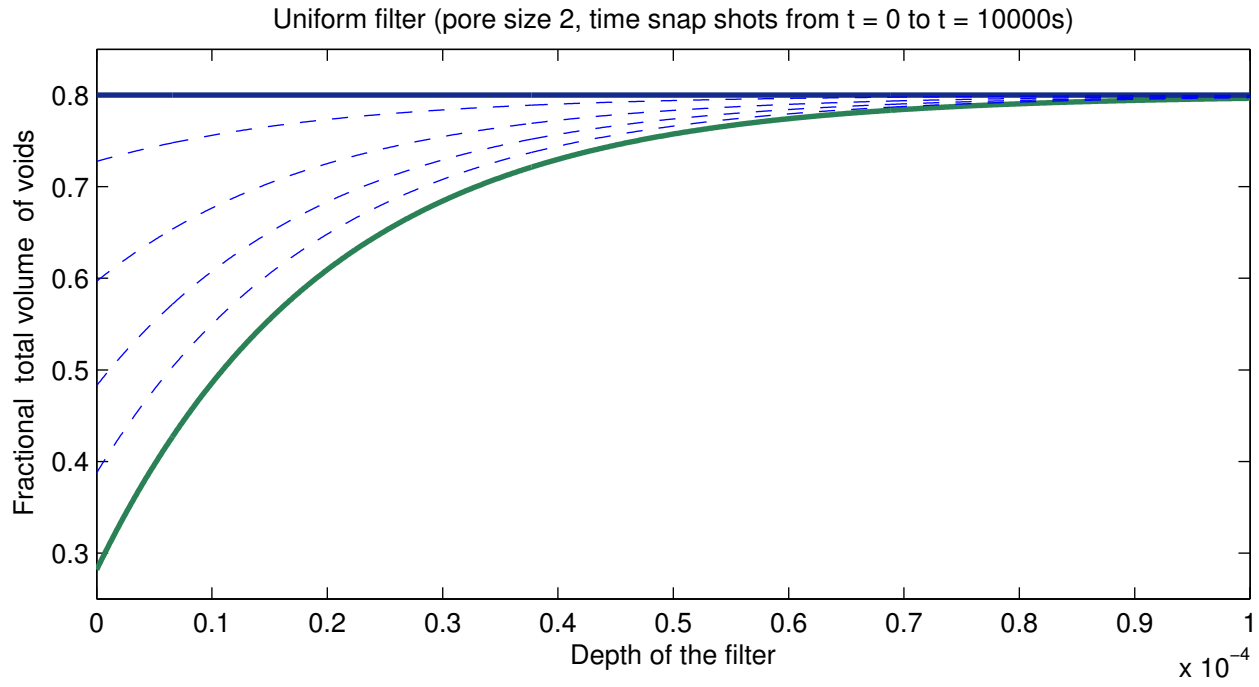

Figure 2: Illustration of the clogging at the top for the uniform filter. Time snapshots of the clogging distribution are shown by dashed lines; these lines become lower as t increases.

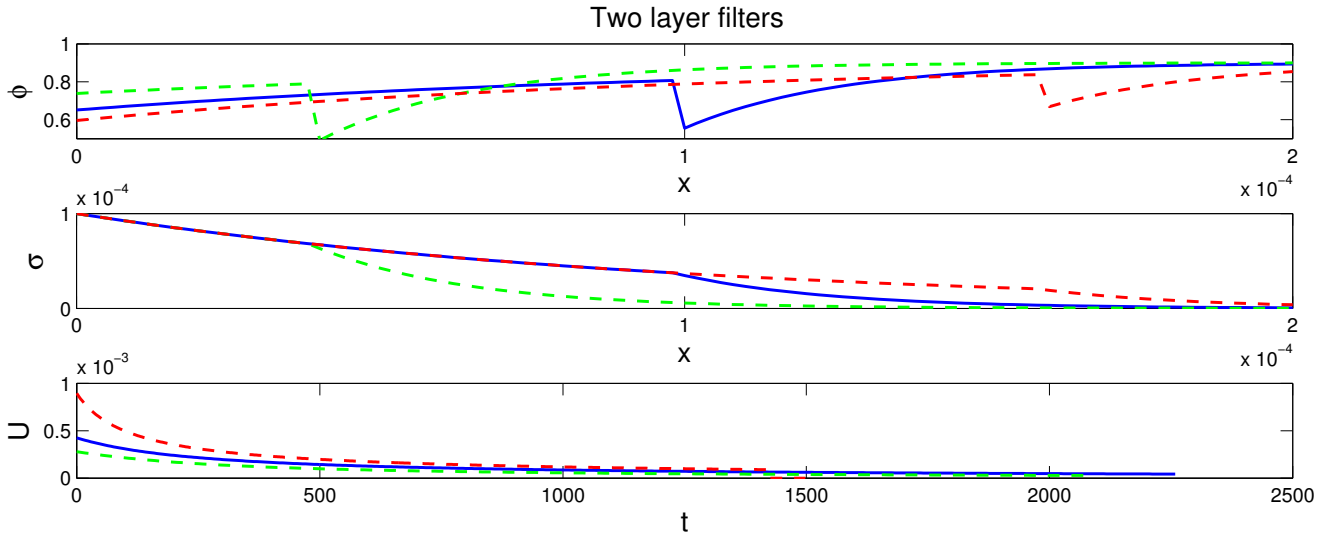

Figure 3: Illustration of more uniform clogging distribution for the two-layer filter.

flow, as above, this may be the filter's lifetime, t_{stop}, defined so that the fluid's flow through the filter at $t = t_{\text{stop}}$ decreases to a given percentage of its initial value (assuming a constant pressure drop). Next, one assigns a set of values to the parameters of the filter's layer i: κ_i (filtration rate), χ_i (constant proportional to d^2 in the permeability K), and depth h_i. Requiring that these parameters be such that the particle concentration at the output of the filter $\sigma(x = h, t \leq t_{\text{stop}})$ is maintained at a given level, one then proceeds to vary them to maximize the filter's lifetime $t_{\text{stop}}[\kappa_i, \chi_i, h_i]$. Of course, making the model more realistic by including particles of different diameters and also the possibility of blocking ("sieving") of the pores by larger particles, is also a possible venue for future study.

It might be interesting to compare performance of filters for different temperature regimes, as a filter configuration for an optimal performance under low temperature might not be a good choice for higher temperatures. Temperature variation affects the governing particulate transport and rate processes in porous media in very complicated ways. Particles tend to deposit more preferentially over the pore surface at lower temperatures than higher temperatures. Hence, colder temperature conditions are favorable for more pore surface attachment and retention of fine particles [3]. Conversely, at sufficiently high temperatures, pore surface conditions become more suitable for particle detachment. Therefore, fine particles are less likely to deposit over the pore surface but rather migrate toward the pore throats and form particle bridges, though only under favorable conditions. The effect of temperature on permeability cannot be neglected because permeability reduction occurs primarily by pore–throat constriction. Even a small increase in temperature can cause sufficient grain expansion to choke the pore–throat openings and to reduce the permeability substantially.

References

[1] F. Civan, "Non-isothermal Permeability Impairment by Fines Migration and Deposition in Porous Media including Dispersive Transport," *Trans. Por. Med.*, vol. 85, pp. 233–258, Oct. 2010.

[2] F. Civan, *Porous Media Transport Phenomena.* Hoboken: Wiley, 2011.

[3] F. Civan, "Temperature effect on power for particle detachment from pore wall described by an arrhenius-type equation," *Trans. Por. Med.*, vol. 67, pp. 329–334, Mar 2007.

Continuum model (Cake model) for the Gore MPI problem

Yixuan Sun, Pejman Sanaei, Linda J. Cummings
New Jersey Institute of Technology, Newark, NJ 07102, USA

1 Introduction

Gore presented a multilayer membrane filter and wants to understand how the "junction" regions between layers affect the filtration performance. These junction regions are created when two layers of materials with different porosities are pressed and connected together to form the multilayer membrane filter. To understand how the junction regions or the porosity profile of the multilayer membrane affects the filtration, we formulated a simple continuum model for the fouling of a variable-porosity membrane in unidirectional flow. This will address Gore's goal to: "Develop a continuum model or framework for characterizing mass transport of species inside of a multilayer porous medium". We call it a cake model as the structures we considered assemble the cake layer formed during the final stage of the filtration.

In figure 1, (a) shows the typical "node-fibril" microstructure of the membrane filter, (b) shows the simplified microstructure where the balls represent the nodes and lines represent the fibers, and (c) is a picture of multilayer membrane structure presented by Gore.

During the MPI workshop we developed an idealized model in which the membrane is viewed as an assembly of identical spheres (the nodes), which provide the surface area for adsorption of particles and thus realizing filtration. The multilayer structure can then be modeled by different packing schemes as indicated in figure 2, where the top layer is packed loosely, representing high porosity and the bottom layer is densely packed which indicates low porosity.

2 Darcy Flow and Fouling Model

We consider dead-end filtration under pressure drop P_0 through a planar membrane that lies parallel to the (Y, Z)-plane, with unidirectional Darcy flow through the membrane in the positive X-direction. The membrane properties and flow are assumed homogeneous in the (Y, Z)-plane, but the membrane has depth-dependent permeability (even if permeability is initially uniform, fouling will lead to nonuniformities over time), which we denote by $K(X, T)$. We use uppercase fonts to denote dimensional quantities.

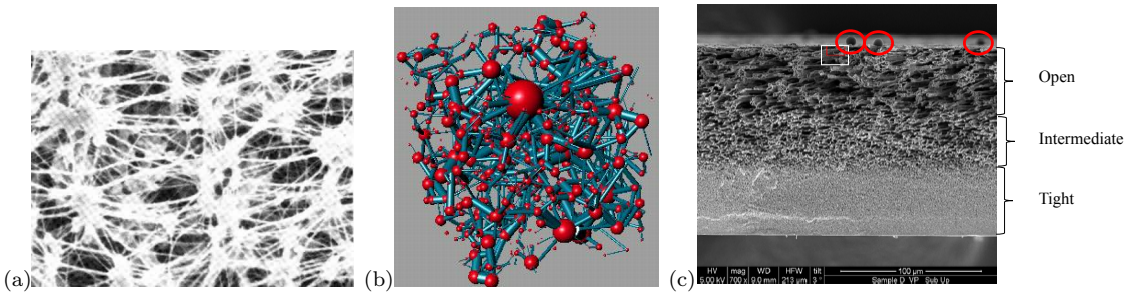

Figure 1: (a) is a picture of the micro structure of a typical membrane filter; (b) is a simplified representation for the micro structure where the balls represent the nodes and lines represent the fibers; (c) is a picture of the multilayer membrane filter presented by Gore.

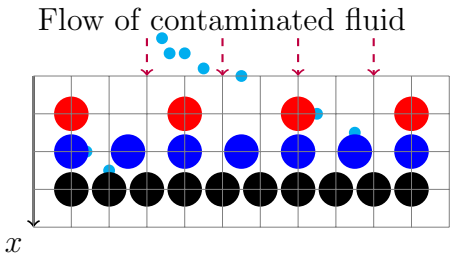

Figure 2: Cake model scheme.

The superficial Darcy velocity $\mathbf{U} = (U(X,T), 0, 0)$ within the membrane is given in terms of the pressure P by

$$U = -\frac{K(X,T)}{\mu}\frac{\partial P}{\partial X}, \quad \frac{\partial}{\partial X}\big(K(X,T)\frac{\partial P}{\partial X}\big) = 0, \quad 0 \le X \le D, \tag{1}$$

$$P(0,T) = P_0, \quad P(D,T) = 0, \tag{2}$$

where D is the membrane thickness and μ is the viscosity of the Newtonian feed solution. The modeling challenge is to link the permeability $K(X,T)$ to membrane characteristics, which evolve in time due to fouling, to obtain a predictive model. We use the Kozeny–Carman equation (see, *e.g.* [5]) to relate its permeability K to its void fraction ϕ:

$$K = \frac{\phi^3}{K_{\text{oz}} S_{\text{cp}}^2 (1-\phi)^2}, \tag{3}$$

where $\phi(X,T)$ is the void fraction or porosity of the cake layers ($\phi \in (0,1)$; for randomly-packed spherical particles for example, $\phi \approx 0.37$); S_{cp} is the specific area (the ratio of the surface area to the volume of the solid fraction of the porous medium); and K_{oz} is the Kozeny constant (Carman proposed a value of 5 in [5]).

The model is completed by making assumptions about how particles are deposited within the membrane. In the spirit of an earlier membrane fouling model for the one-layer membrane

filter [8], we propose a simple advection model for the small particles:

$$U_{\mathrm{p}}\frac{\partial C}{\partial X} = -\Lambda\frac{C}{(\phi\Delta_{\mathrm{p}})^{1/3}}. \tag{4}$$

Here the pore velocity U_{p} within the membrane is related to the superficial Darcy velocity U by $U_{\mathrm{p}} = \frac{U}{\phi}$.

As in [8], the model assumes that small particles are deposited at a rate proportional to the local particle concentration. The constant Λ captures the physics of the attraction between the large particles (nodes) and the small particles (contaminants). In essence, the pores of the membrane consist of the spaces between nodes of volume Δ_{p}; therefore we assume that $(\phi\Delta_{\mathrm{p}})^{1/3}$ will be proportional to the pore radius. The membrane porosity ϕ decreases in response to the particle deposition: consistent with [8] (with pore radius A taken proportional to $(\phi\Delta_{\mathrm{p}})^{1/3}$) we propose

$$\frac{\partial\phi}{\partial T} = -\Lambda(\phi\Delta_{\mathrm{p}})^{2/3}C. \tag{5}$$

3 Scaling and nondimensionalization

We nondimensionalize the model presented above using the scalings

$$X = Dx, \quad T = \frac{1}{\Lambda\Delta_{\mathrm{p}}^{2/3}C_0}t, \quad (U, U_{\mathrm{p}}) = \frac{P_0}{\mu D K_{\mathrm{oz}} S_{\mathrm{cp}}^2}(u, u_{\mathrm{p}}),$$

$$P = P_0 p, \quad C = C_0 c, \quad K = \frac{1}{K_{\mathrm{oz}}S_{\mathrm{cp}}^2}k, \tag{6}$$

giving a dimensionless model for $u(x,t)$, $u_{\mathrm{p}}(x,t)$, $p(x,t)$ $a(x,t)$, $c(x,t)$ and $\phi(t)$. The dimensionless governing equations in the membrane layer $0 \le x \le 1$ are

$$u = -k\frac{\partial p}{\partial x}, \quad \frac{\partial u}{\partial x} = 0, \tag{7}$$

$$k = \frac{\phi^3}{(1-\phi)^2}, \tag{8}$$

$$\frac{\partial\phi}{\partial t} = -c\phi^{2/3}, \tag{9}$$

$$u\frac{\partial c}{\partial x} = -\alpha c\phi^{2/3}, \quad \alpha = \frac{\Lambda\mu D^2 K_{\mathrm{oz}} S_{\mathrm{cp}}^2}{P_0 {\Delta_p}^{1/3}}, \tag{10}$$

with boundary and initial conditions

$$p(0,t) = 1, \quad p(1,t) = 0, \quad c(0,t) = 1. \tag{11}$$

The above implicitly assumes that the specific area, S_{cp}, is constant throughout. This will not quite be true, but we believe it is reasonable to neglect its evolution due to fouling.

4 Results and Discussion

Equations (7) and (11) give the following analytic solution for p:

$$p = 1 - \frac{\int_0^x \frac{1}{k}\, d\tilde{x}}{\int_0^1 \frac{1}{k}\, d\tilde{x}}. \tag{12}$$

From equation (7) we find u is a function of time only:

$$u = \frac{1}{\int_0^1 \frac{1}{k}\, d\tilde{x}}. \tag{13}$$

From the above analytic solutions for p and u we find the following system of equations:

$$\frac{\partial c}{\partial x} = -\alpha c \phi^{\frac{2}{3}} \int_0^1 \frac{1}{k}\, d\tilde{x}, \quad k = \frac{\phi^3}{(1-\phi)^2}, \tag{14}$$

$$\frac{\partial \phi}{\partial t} = -\phi^{\frac{2}{3}} c. \tag{15}$$

We have the following BC and IC:

$$c(0,t) = 1; \qquad \phi(x,0) = \phi_0(x). \tag{16}$$

Gore provided an initial profile for a simple two-layer member filter. Each layer has width about 0.45 in our length scale, with a middle layer connecting the two layers with different porosities. The middle layer (connecting layer) has length scale 0.1, which may have yet a third porosity, depending on the pressing and the material properties of the two layers (see Fig. 3(a)).

There are different ways to evaluate the performance of filters; in this study we use throughput and outlet particle concentration. The throughput measures how much fluid can be processed before the membrane is completely clogged. The concentration at the outlet measures how effective the filtration is. Here we consider the filtration is effective if 90% of the particles are removed, *i.e.*, the concentration at the outlet should be below 0.1 for feed solution of concentration 1. Figures 3(b,c) show how throughput and concentration change by varying ϕ_m (see Fig. 3(a)), the porosity of the middle "junction" layer, from 0.1 to 0.5. From Figure 3(b) we can see that when $\alpha = 1$, increasing the porosity will increase the throughput, which is a quantity we want to maximize. For small α (0.1 in Fig. 3(c)), increasing the porosity of the middle layer will increase the throughput, but the filtration becomes ineffective as soon as $\phi_m > 0.15$. This simulation indicates the optimization of the porosity profile of multilayer membrane filters depends on the constant Λ and other parameters that can affect α, such as applied pressure P_0, viscosity μ, and membrane depth D as indicated by (10). These quantities allow us to manipulate α to achieve the optimized filtration based on the application.

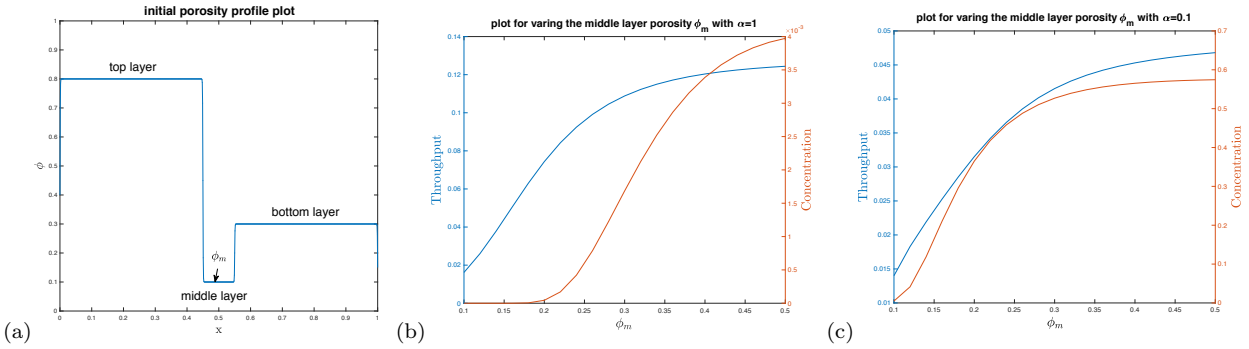

Figure 3: (a) Porosity profile with ϕ_m being indicated for the middle layer; (b) plot for varying the middle layer porosity ϕ_m with $\alpha = 1$; (c) plot for varying the middle layer porosity ϕ_m with $\alpha = 0.1$.

5 Conclusions and Future Study

In this study, we began to formulate an optimization problem based on our continuum model. The optimization depends on the application, *i.e.*, the definition of effective filtration may be desired to be 99.99% particle removal in some applications, while for other situations 90% removal is effective. Under different constraints, one may be able to select an optimized filter which maximizes the throughput under given conditions, *i.e.*, for fixed α, by varying the porosity profile of the membrane filter; or given the fixed profile of porosity, some α will give the highest throughput, which is yet another type of optimization. With guidance from Gore, we believe we will be able to carry out optimization of our model. We also plan to refine our model to account for (i) changes in specific area S_{cp} due to fouling; and (ii) changes in node size Δ_{p} with membrane depth. If time permits we also plan to compare our results to those from an alternative model based on homogenization theory [2]. One of the authors of that study has agreed to run simulations of that model to compare with our model results. I would also like to compare our results with the discrete network model, and another continuum model that MPI group member Binan Gu worked on. We would like to publish our findings in a peer-reviewed journal within one year.

References

[1] Dalwadi, M.P., Griffiths, I. M., Bruna, M. Understanding how porosity gradients can make a better filter using homogenization theory. *Proc. R. Soc. A.* **471**, 2182 (2015).

[2] Dalwadi, M. P.,Bruna, M., Griffiths, I. M. A multiscale method to calculate filter blockage. *J. Fluid Mech* **809**, 264-289 (2016).

[3] Griffiths, I. M., Kumar, A., Stewart, P. S. A combined network model for membrane fouling. *J. Coll. Int. Sci.* **432**, 10-18 (2014).

[4] Polyakov, Y.S. Depth filtration approach to the theory of standard blocking: Prediction of membrane permeation rate and selectivity. *J. Membrane Sci.* **322**, 81-90 (2008).

[5] Probstein, R. Physicochemical Hydrodynamics, An Introduction, Second Edition. Wiley Interscience (1994).

[6] Pujar, N.S., Zydney, A.L. Charge regulation and electrostatic interactions for a spherical particle in a cylindrical pore. *J. Colloid Interface Sci.* **192**, 338-349 (1997).

[7] Sanaei, P., Richardson, G. W., Witelski, T., Cummings, L. J. Flow and fouling in a pleated membrane filter. *J. Fluid Mechanics.* **795**, 36-59 (2016).

[8] Sanaei, P., Cummings, L. J. Flow and fouling in membrane filters: Effects of membrane morphology. *J. Fluid Mechanics.* **818**, 744-771 (2017).